

A weak El Niño-Southern Oscillation with a delayed growth phase around 4,300 years ago

H.V. McGregor, M.J. Fischer, M.K. Gagan, D. Fink, S.J. Phipps, H. Wong, C.D. Woodroffe

Supplementary Methods
Supplementary Discussion
Supplementary Figures 1-11
Supplementary Tables 1-6
Supplementary References

Corresponding author: H.V. McGregor, School of Earth and Environmental Sciences, University of Wollongong, NSW 2522, Australia. Email: mcgregor@uow.edu.au, mcgregor@uni-bremen.de
Telephone: +61 2 4221 4265, Fax: +61 2 4221 4250

Supplementary methods

Coral collection and setting

Kiritimati Island, in the central Pacific Ocean (Supplementary Figure 1), is a low-lying atoll surrounded by a narrow reef flat (typically 80 m), and the interior contains a network of hypersaline lakes. Rainfall at Kiritimati Island is low (2 mm/day for 1982–2007; Adler et al., 2003), except during El Niño events when rainfall increases dramatically (e.g. austral summer 1997/1998 the rate was 11.4 mm/day; Adler et al., 2003). Mean SST over the period 1982–2007 was 27.4 ± 1.2 (1σ) °C for the $1^\circ \times 1^\circ$ grid square including Kiritimati Island, with the SST minima occurring in early February, and the maxima occurring in June (Reynolds et al., 2002). SST anomalies of up to 3 °C in the boreal winter are recorded during El Niño events, and SSTs can be 1–2 °C cooler than average during La Niña events (Wyrski, 1975).

Fossil *Porites* sp. coral microatoll XM35 grew to a remarkable ~5 m in diameter, and a radial slab was collected from the coral in 2007. XM35 occurs in the position in which it grew, on a reef amongst a range of associated branching *Acropora* corals and *Tridacna*, beside what is now a hypersaline lake, one of many in the Mouakena Closed Area at the southeast of Kiritimati Island (01°44.212'N, 157°12.522'E). Dating of *Porites* microatolls and associated biota, together with geomorphic investigations, indicate that the interior of the Island was a flourishing reef growing uninterrupted between 6400 and 1500 years BP (Woodroffe and McLean, 1998; McGregor et al., 2011b). Microatolls aged between 1500 years BP to present have not been found in the interior suggesting that the area has not been suitable for microatolls since then. The present-day lagoon does not appear to be the analogous environment for XM35 as *Porites* microatolls have not been found in that setting. Instead, living Kiritimati *Porites* microatolls today are found on well-flushed, active reef flats on the fringe of the Island (McGregor et al., 2011a; McGregor et al., 2011b). Finally, preliminary measurements of SST in a variety of reef settings across the Island (active reef flats with living microatolls, lagoon entrance, and shallow settings within the lagoon (no microatoll growth)) suggest that absolute SSTs vary by ~0.5 °C and the SST amplitudes are very similar. This suggests remarkable SST consistency, regardless of the reefal setting, and that our fossil coral is likely a faithful recorder of climate and ENSO variations for the time it was alive.

Screening for diagenesis

Fossil coral XM35 was screened for diagenesis using X-ray diffraction (XRD) and petrographic analysis. Two ~7mm slices were cut from XM35. One slice was used for geochemical analysis, and from the parallel slice one block (~3x4 cm) was cut approximately every 20 cm from the outer to the inner margins of the coral. Blocks were sub-sampled with the first portion used for XRD analysis to screen for calcite and the second portion used to prepare a thin section to screen for calcite, secondary aragonite, dissolution, and other post-depositional textures (McGregor and Abram, 2008). Both portions were thoroughly cleaned using RiOS water and a Branson 450 ultrasonic probe.

Samples for XRD were crushed to a fine powder under ethanol with a mortar and pestle. XRD samples were measured on a Phillips Goniometer with a Spellman DR3 Copper X-ray generator run at 1 kV, and scanned at 2° per minute for a 2θ range of 4–70°. The percent aragonite and calcite in each sample was estimated using SIROQUANT version 3 software utilising the Rietvelt method for analysing diffraction peaks. All samples contained $\leq 0.2\%$ calcite (Supplementary Table 1), and the

coral was rated as excellent preservation (Supplementary Fig. 2), based on thin section analysis and the criteria of McGregor and Abram (2008).

X-radiography, and sampling along maximum growth axis

A ~7 mm slice was taken from the XM35 section and X-rayed to reveal the coral density bands, which show horizontal growth towards the coral's outer margins (Supplementary Fig. 3). The ~7 mm slice was reduced to a ~2 mm ledge, thoroughly cleaned using MilliQ water and a Branson 450 ultrasonic probe, and dried in an oven set to 40°C for 24 hours. The ~2 mm ledge was then continuously microsampled along the major growth axis (Supplementary Fig. 3) at equivalent to fortnightly sampling, using a low-speed milling system (Gagan et al., 1994). Annual growth bands revealed by X-radiography and stable isotope analyses show that XM35 has an average growth rate of 15 mm/year, and provides a ~175 year "window" into ENSO variability during the time through which it lived.

U-series age dating

A small coral piece from section XM35-H1 (Supplementary Fig. 3), equivalent to approximately year 130 of the coral's internal chronology, was thoroughly cleaned in MilliQ water and by ultrasonic probe in preparation for U-Th age dating. Two 50–100 mg aliquots were weighed out, prepared and measured at the Radiogenic Isotope Laboratory, University of Queensland following the procedures outlined in Zhou et al. (2011). In summary, the aliquots were dissolved in nitric acid and spiked with a ^{229}Th - ^{233}U mixed tracer. Following chemical separation, a mixed U-Th solution was made such that the final 3 ml solution had a U concentration of ~10 ppb or less. U-Th isotopic ratio measurement was performed on the Nu Plasma multi-collector inductively coupled plasma mass spectrometry (MC-ICP-MS) following the analytical protocol described by Hellstrom (2003), with minor modifications (Zhou et al. 2011). The $^{238}\text{U}/^{235}\text{U}$ value of 137.88 was used for mass fractionation correction for both U and Th isotopic ratio measurements. Monitoring of carryover memories showed that ^{230}Th memory was consistently less than 0.1 count s^{-1} , and was negligible for all other isotopes. U-Th ages were calculated using the Isoplot/EX 3.0 program (Ludwig, 2003).

$(^{234}\text{U}/^{238}\text{U})_{\text{initial}}$ values for both dates are within the acceptance criteria of 1.1455 ± 0.0023 based on values for Holocene seawater (Supplementary Table 2; Cheng et al., 2000). The U-Th ages quoted in yBP were calculated relative to 1950 AD (Supplementary Table 2). A random effects model (Galbraith and Laslett, 1993; Galbraith et al., 1999) was used to calculate a weighted mean calendar age and standard error of the two U-series aliquots, and was taken as the U-series age of the coral. This weighting and standard error calculation takes into account the 2σ errors on each individual age date. The weighted average coral U-series age is $4,243 \pm 9$ yBP (Supplementary Table 2). Taking into account the location of the U-series dating sample within the coral, and the years of coral growth, the XM35 coral lived between 4,400 and 4,200 years ago, with an average age of ~4.3 kyBP.

$\delta^{18}\text{O}$ analysis

Coral $\delta^{18}\text{O}$ on fossil coral XM35 was measured at approximately monthly resolution on a Finnigan MAT 251 mass spectrometer. For each sample aliquot, 200 ± 20 μg of powder was initially dissolved in 105% H_3PO_4 at 90°C in an automated carbonate (Kiel) device. Isotope results were calibrated relative to the Vienna Peedee Belemnite (v-pdb) using the NBS-19 ($\delta^{18}\text{O} = -2.20\text{‰}$) and

NBS-18 ($\delta^{18}\text{O} = -23.0\text{‰}$) standards. The standard deviation for in-run $\delta^{18}\text{O}$ measurements on NBS-19 ($n = 329$) was 0.04‰ during the course of the analysis. The average standard error for replicate $\delta^{18}\text{O}$ measurements for coral samples is 0.04‰ ($n = 100$). The mean $\delta^{18}\text{O}$ value for XM35 ($-4.77 \pm 0.15 \text{‰}$) is within the range of modern values for the stacked modern $\delta^{18}\text{O}$ record (Fig. 1 and Supplementary Fig. 4).

Coral time-series age model

The time-series for coral XM35 was established in the same way as for the modern coral microatoll record (XM22) as described in McGregor et al. (2011a) by assigning XM35 $\delta^{18}\text{O}$ maxima to early February using the Analyseries software package (Paillard et al., 1996) and taking into account the average coral growth rate (15 mm/year). Model results support a February climatological SST minimum. The CSIRO Mk3L climate system model (Phipps et al., 2011, 2012) was used to conduct a pre-industrial control simulation and three transient simulations of the past 8 ka. The transient simulations were forced with changes in the Earth's orbital geometry only. Climatological SSTs were derived from the control simulation, and from the period 5-4 ka of the transient simulations. In both cases, February was the coldest month of the year at the location of Kiritimati Island. The possible effect of shifting the monthly tie-point by ± 1 month on the results presented in this paper is discussed in the Supplementary Discussion.

On rare occasions where a $\delta^{18}\text{O}$ maximum was poorly resolved in the coral no tie-point was assigned. The age model was interpolated between the previous year February tie-point and the subsequent year February tie-point, and was checked against the density bands in x-ray and the coral growth rate to verify the number of years between the two tie-points.

Approximately 10 months (February-November) were missing from one year in XM35 coral section R1 (Supplementary Fig. 3). These data were recorded as NaN in the raw data file. For the statistical calculations values were linearly interpolated between January and December. Data missing from this one partial year are unlikely to affect ENSO and annual cycle changes calculated based on this coral.

The $\delta^{18}\text{O}$ data were interpolated using ARAND software (Howell et al., 2006) to give 12 values/year.

The overall age model error on the coral time-series is estimated as ± 1 year.

Sr/Ca analysis

Coral Sr/Ca was measured on the youngest 30 years of coral microatoll XM35, and for 1994-2007 in modern coral microatoll XM22 to verify the dominant contribution of SST to Kiritimati coral $\delta^{18}\text{O}$ in non-El Niño years (Supplementary Discussion). Aliquots of 0.55 ± 0.5 mg from the same coral samples as for $\delta^{18}\text{O}$ were weighed into pre-cleaned centrifuge tubes and dissolved in 1% (vol/vol) HNO_3 . For each sample the volume of acid was added to give a Ca concentration of 40 ± 4 ppm for each dissolute sample. The tubes were shaken manually and placed in a 40°C sonicator bath for 30 minutes to completely dissolve the coralline aragonite.

Samples were measured on a Varian (VISTA AX - Charged Coupled Device Simultaneous) ICP-AES, calibrated using a standard solution series containing Sr, Ba, P and Mg in a range of different concentrations and with a 40ppm Ca matrix. Blank 1% HNO_3 samples were measured at the start of each run and periodically throughout the run. A reference solution was measured after every sample

or after every second sample, and was used for offline correction for instrument drift. The resulting within-run precision was ± 0.02 mmol/mol (0.2% RSD). The JCp-1 coral reference material (Okai et al., 2002) was included in every run and the standard deviation for repeat measurements was ± 0.03 mmol/mol ($n = 24$). The average standard error for repeat analyses of Sr/Ca sample solutions was 0.005 mmol/mol ($n = 56$).

The coral $\delta^{18}\text{O}$ -based age model also applies to the Sr/Ca results, since the Sr/Ca analyses were performed on the same coral powders.

Methods for statistical calculations for Figures 1-4 and Supplementary Table 3

The main *Data* records analysed in this paper are:

- 1) Kiritimati SST March 1938 to May 2007 (from ERSSTv3b SSTs (Smith et al., 2008) for 158°W, 2°N, and includes Kiritimati Island)
- 2) Kiritimati modern coral $\delta^{18}\text{O}$ stack, March 1938 to May 2007 (Supplementary Figure 4)
- 3) WM_stack Kiritimati modern coral $\delta^{18}\text{O}$ stack, February 1978 to May 2007 (Supplementary Figure 4)
- 4) The ~4.3 kyBP (XM35) coral $\delta^{18}\text{O}$ record

These data series were broken down into three component time series (*Trend*, *Annual*, and *Residual*), such that:

$$Data = Trend + Annual + Residual \quad (1)$$

The *Trend* series was modelled using a penalized regression spline with smoothing parameters estimated by generalized cross-validation (Wood, 2006).

The *Annual* series was modelled using a monthly indicator matrix,

$$I_{i,m} \begin{cases} 0 \\ 1, \text{ when } i = m \end{cases}$$

where $m = 1:12$ (columns), $i = n \bmod 12$, $n = 1$ to N , $N =$ total number of months (rows).

The *Residual* series was extracted as the *Data* minus (*Trend+Annual*) series (i.e. detrended and deseasonalised). The *Residual* series are dominated by the interannual (ENSO) variability (Supplementary Fig. 5), and hence the *Residual* series are also referred to as the ‘interannual time series’ in the text.

The formulation of equation (1) allows the trend and seasonality to be simultaneously estimated from the data using multivariate regression (by generalized additive modelling).

The raw data for all three time series, and the WM_stack, separate into distinct *Trend*, *Annual* and *Residual* (interannual) spectral bins (Supplementary Fig. 5). Note that for Fig. 1d the spectral analysis was performed on the Residual (interannual) time series only.

The various components calculated using equation (1) are described in more detail below and are plotted as follows:

- Figure 1: The *Data* series are plotted in Figure 1a-c. Figure 1a-c also shows the 2-8 year Butterworth band pass filter of the *Data* plus the *Trend* for each record. Figure 1d shows the spectral analysis of the *Residual* (interannual) time series.
- Figure 2a-c: The *Residual* (interannual) time series are plotted in 2a-c, with additional cluster analysis of the time series used to divide the interannual time series into El Niño (red), La Niña (blue) and neutral (black) years.
- Figure 2d-f: Results from the cluster analysis of the *Residual* (interannual) time series plotted in Figure 2a-c were used to produce a composite picture of the seasonal evolution of El Niño, La Niña and neutral years for each record and are plotted in Figure 2d-f.
- Figure 3: The average *Annual* series for WM_stack $\delta^{18}\text{O}$ and Kiritimati SST for 1978-2007, and for ~4.3 kyBP coral $\delta^{18}\text{O}$, excluding strong El Niño years, are plotted in Figure 3a as average annual cycles. The March 1938 to May 2007 modern coral $\delta^{18}\text{O}$ stack was not used for reconstructing the average *Annual* series to avoid possible biases due to the 1-2 month 'spawning spikes' in the Evans et al. (1998) coral $\delta^{18}\text{O}$ record. For WM_stack $\delta^{18}\text{O}$ and Kiritimati SST the El Niño years (July-June) 1982-1983, 1986-1987, and 1997-1998 were excluded from the analysis to avoid possible biases due to additional rainfall contributions to the $\delta^{18}\text{O}$ seawater. For the ~4.3 kyBP coral years (July-June) 21-22, 26-27, 52-53, 76-77, 88-89, 121-122, 140-141, and 170-171 were excluded.
- Figure 4: Running 21-year variance of the JFM anomaly was extracted from the *Residual* (interannual) time series.
- Supplementary Table 3 and Supplementary Figure 6: The *Data* series were filtered into annual and Interannual bands and the ratio of variance explained by each band was plotted in Supplementary Figure 6.

Spectral analysis – Figure 1d:

The power spectral density (S) of each *Residual* (interannual) time series was estimated using the multitaper method (MTM; Ghil et al., 2002). MTM reduces the variance in the spectral estimate by pre-multiplying the time series with orthogonal tapers. The number of tapers (K) and the bandwidth parameter (p) were set at $K=3$ and $p=2$, which is suitable for time series that have a length N of a few hundred time points (Ghil et al., 2002). The theoretical spectrum and 95% confidence interval for the 'red noise' null hypothesis were calculated for the Kiritimati modern coral $\delta^{18}\text{O}$ stack (Gilman et al., 1963; Ghil et al., 2002). Power spectra for Kiritimati SST and the ~4.3 kyBP coral $\delta^{18}\text{O}$ record were calculated on the interannual time series for moving 69-year windows, using a 1-month sliding time step. The median, 2.5 and 97.5% quantiles of spectral power are plotted in Fig. 1d.

Slight differences between the Kiritimati SST and modern coral $\delta^{18}\text{O}$ stack in Figure 1d are due to the different time intervals used to calculate the spectra. When the spectra are calculated for the same interval (1938-2007) both display typical bimodal 'modern' ENSO spectrum (not shown), characterised by peaks at ~2.5, 3.6 and 5.3 years (Moron et al., 1998).

Note that the power spectra in Figure 1 are based on the interannual (residual) time series only (i.e. all records detrended and deseasonalized) so as to best highlight differences between the modern and fossil interannual power. This is in contrast to Supplementary Figure 5, where the

spectra are calculated on the three component time series, to demonstrate that the annual, interannual, and trend components fall into distinct frequency ‘bins’. Note also that the y-axis is different in Supplementary Figure 5 and Figure 1d for clearer comparison of the spectra of the different components.

Cluster Analysis – Figure 2a-c:

In order to investigate changes in ENSO amplitude, phase and symmetry we used cluster analysis to classify (cluster) the *Residual* (interannual) time series into El Niño years, neutral years, and La Niña years. The method has the advantage for studying mid-Holocene ENSO in that it does not require a preconceived definition of an El Niño or La Niña event, a useful trait given that El Niño events could have a different temporal structure in the mid-Holocene.

Time series cluster analysis was performed using a K-means algorithm (Hartigan and Wong, 1979). K-means is a partitioning algorithm that divides the data into a pre-specified number of groups, g , that are both internally homogenous and externally separated from one another (as much as possible). K-means partitions data on the basis of multiple features, including the shape, phase and amplitude of events, and these features are known to be an important characteristic of ENSO events. K-means uses all the important information available in the time series matrix to define the clusters (anomaly size, shape etc.), whereas threshold definitions use only part of the available information (anomaly size). K-means always finds partitions in a dataset.

K-means minimizes:

$$SS_{W_i} = \sum_{j=1}^m (Y_{ij} - \bar{Y}_i)^2 \quad \text{(Within-cluster sum of squares)} \quad (2a)$$

$$\bar{Y}_i = m^{-1} \sum_{j=1}^m (Y_{ij}) \quad \text{(Group means)} \quad (2b)$$

To test the statistical significance of the group means, we also need:

$$SS_T = \sum_{i=1}^g \sum_{j=1}^m (Y_{ij} - \bar{Y}_{..})^2 \quad \text{(Total sum of squares)} \quad (2c)$$

$$\bar{Y}_{..} = (mg)^{-1} \sum_{i=1}^g \sum_{j=1}^m Y_{ij} \quad \text{(Grand mean)} \quad (2d)$$

$$SS_W / SS_T = SS_T^{-1} \sum_{i=1}^g SS_{W_i} \quad \text{(Ratio of } SS_W:SS_T) \quad (2e)$$

To implement K-means, each *Residual* (interannual) time series was arranged into an array where rows = years, and columns = months (July-June). Specifying $g=3$ groups allows K-means to naturally partition, for example, the SST data into positive (El-Niño), negative (La-Niña) and neutral ‘years’. K-means was implemented with 20 random starts, which helps avoid local minima in the objective function. The results are shown in Figure 2.

Note prior to cluster analysis of the stacked modern coral $\delta^{18}\text{O}$ record the positive ‘spawning spikes’ from the Evans et al. (1998) coral record were identified and removed by performing a median smoothing of the stacked $\delta^{18}\text{O}$ record, calculating the 99th percentile of the negative anomalies of the median smoothed record, then applying this to the positive anomalies and removing any positive anomaly outside the 99th percentile. This procedure did not change the number of years in the modern $\delta^{18}\text{O}$ stack identified as positive, negative or neutral years, nor change the cluster composites in Figure 2.

The statistical significance of the clusters was tested using Linear Discriminant Analysis (LDA) and a MANOVA test (using Wilks’ lambda). Wilks’ lambda is the determinant of the within-cluster sum of squares (SS_w) divided by the determinant of the total sum of squares (SS_T). Wilks’ lambda has values between 0-1, whereby small values correspond to a large difference between the clusters. For the three *Residual* (interannual) time series, the actual ratio $SS_w:SS_T$ was 0.2 (Kiritimati SST 1939-2007), 0.24 (Kiritimati modern coral $\delta^{18}\text{O}$ stack 1939-2007) and 0.26 (~4.3 kyBP coral). All these ratios are statistically significant (MANOVA test using Wilks’ lambda). Thus the negative and positive anomaly years identified by cluster analysis of the XM35 record do indeed characterise the development of El Niño and La Niña events during the mid-Holocene compared to the present day.

We test the skill of the cluster analysis against five commonly-used ENSO indices (Supplementary Tables 4 and 5). The cluster analysis is applied to the ERSSTv3b NINO3.4 SST (Smith et al. 2008). The five ENSO indices all use different criteria to define events leading to discrepancies among the indices as to what is and is not an El Niño or La Niña year. We first assess the agreement between the ENSO indices by calculating the percentage of indices that record an El Niño year (Supplementary Table 4), and the percentage that record a La Niña year (Supplementary Table 5). If the cluster analysis shows an event in a given year, yet <50% of ENSO indices record an event in that same year the event is recorded as a false positive. If >50% of ENSO indices show an event yet the cluster analysis does not then that event is recorded as a false negative. Post-1950 there are three false negative El Niño events (1951, 1953, 1993) and one false positive La Niña event (1967). Prior to 1950 there are: no false negative El Niño events; five false positive El Niño events (1884, 1885, 1904, 1929, 1940); four false negative La Niña events (1878, 1890, 1897, 1906); two false positive La Niña events (1908, 1944). Note that the ENSO indices definitions of El Niño and La Niña events pre-1950 are based on the Southern-Oscillation Index and the threshold/EOF-based index of Meyers et al. (2007), where the input data are less reliable, rather than NINO3.4 threshold indices (the latter are more relevant to our central Pacific coral site). Note too that the terms ‘false positive’ and ‘false negative’ assume that the other ENSO indices correctly identify events, which particularly in the early part of the record may not be the case. Overall, the cluster analysis records the majority of El Niño and La Niña events seen in the ENSO indices and can be considered equal to the earlier indices of ENSO.

Cluster analysis interannual time series composites – Figure 2d-f:

The cluster composites (with confidence intervals) are plotted in Figure 2d-f. For the modern coral $\delta^{18}\text{O}$ stack (2e), the cluster composites were calculated by fitting a generalised additive model to all years (July-June) within each cluster, i.e. the regression spline is a smoothed function of the months (with smoothing parameters estimated by cross-validation). These cluster composites are essentially the same as the cluster centres calculated by the K-means algorithm. For the instrumental SST anomaly (1877-2007) and XM35 anomaly time series, the k-means cluster analysis

was performed separately for 69-year windows, using a 1-year time step and July-June years. The cluster means were calculated for each window, and the set of these cluster means was used to generate the median, 2.5 and 97.5% quantiles in Figures 2d and 2f. For the modern coral $\delta^{18}\text{O}$ stack there is only one 69-year window (1938-2007) so the 95% confidence intervals are calculated using standard errors of the mean.

Mean annual cycle – Figure 3a:

The mean annual cycles for different records (WM_stack $\delta^{18}\text{O}$ and Kiritimati SST, and XM35 $\delta^{18}\text{O}$) were determined from the *Annual* component time series (equation 1) excluding strong El Niño years. The March 1938 to May 2007 modern coral $\delta^{18}\text{O}$ stack was not used for reconstructing the average annual cycle to avoid possible biases due to the 1-2 month ‘spawning spikes’ in the Evans et al. (1998) coral $\delta^{18}\text{O}$ record, and diagenesis in the Nurhati et al. (2009) record LaVigne et al. (In press) Instead we used the WM_stack $\delta^{18}\text{O}$ (Supplementary Fig. 4) based on Woodroffe et al. (2003) and McGregor et al. (2011a).

For WM_stack $\delta^{18}\text{O}$ and Kiritimati SST the strong El Niño years July 1982 – June 1983, July 1987 – June 1988, and July 1997 – June 1998 were excluded from the analysis to avoid possible biases due to rainfall contributions to the $\delta^{18}\text{O}$ seawater. For the ~ 4.3 kyBP coral years July 21 – June 22, July 26 – June 27, July 52 – June 53, July 76 – June 77, July 88 – June 89, July 121 – June 122, July 140 – June 141, and July 170 – June 171 were excluded.

For the detrended instrumental SST (1877-2007) and XM35 time series, the annual cycle was calculated for the full record length using a 29-year (348-month) window, with a 1-month time step. A 29-year window length was used to match the length of the WM_stack $\delta^{18}\text{O}$. These mean annual cycles are plotted in Figure 3a.

The errors on the estimate of the mean annual cycle amplitude for the WM_stack and ~ 4.3 kyBP coral are a confidence interval calculated by applying a bootstrap method to the individual time series. First, the individual time series were arranged into a time matrix with 12 columns (corresponding to months) and rows corresponding to years. Next, whole rows were randomly selected from the time matrix, until a new matrix of the same size is formed. The new matrix was then unfolded to form the bootstrapped time series. Thus, each bootstrapped time series consists of fixed 12-month blocks of the original time series, randomly selected (with replacement), and randomly ordered. For each bootstrapped time series, the annual cycle amplitude was calculated using regression with monthly indicator matrix, as described at the beginning of the Supplementary Methods for Statistical Calculation section. The process was repeated using 2000 bootstrapped realisations, and from the probability distribution function (pdf) of the annual cycle amplitude the standard deviation (and confidence interval) was calculated.

Applying this method to the modern WM_stack and the fossil ~ 4.3 kyBP coral gives:

WM_stack annual amplitude = $0.17 \pm 0.06\%$

XM35 annual amplitude = $0.22 \pm 0.02 \%$

(The values here are the bootstrap-estimated 2 standard deviation error).

The above results show that the mean annual amplitude in the modern WM_stack (0.17‰) falls outside the 95% confidence interval for the ~ 4.3 kyBP coral annual cycle amplitude (0.205-

0.239‰). Although the reverse is not true (WM_stack 0.11-0.23‰, 95% confidence interval), this comparison does not constitute a proper test of the null hypothesis “that there is no difference in the annual cycle amplitude of two time series”. A test of this null hypothesis is described in the Supplementary Discussion and demonstrates that the amplitudes of the annual cycles in the ~4.3 kyBP and modern corals are different.

Running 21-year variance of the interannual time series – Figure 4:

The interannual (*Residual*) time series are detrended and deseasonalised, so after calculating the mean anomaly for the months JFM for each year, the running standard deviation (σ) is simply the square root of the mean squared JFM anomaly, calculated in 21-yr windows. The 21-year running standard deviation of boreal winter anomalies are used in order to investigate interdecadal modulation of ENSO amplitude (Fig. 4). Interdecadal modulation (i.e. >10 years) is an important feature of ENSO in observational and modelling studies (Fang et al., 2008; Soon-Il, 2009; Li et al., 2011; Yu and Kim, 2011). These studies all report: (i) interdecadal modulation of ENSO amplitude at 9-15 year timescales, and (ii) that there are two main patterns of interdecadal ENSO modulation, commonly referred to as PDV1 and PDV2 (Pacific Decadal Variability 1 and 2). So the 21-yr window length is neither too long nor too short relative to the 9-15 year timescale of interdecadal ENSO modulation, and hence we can compare our results with other published works.

The confidence intervals on the plots are 95% confidence intervals (2.5/97.5%) for the null hypothesis of ‘randomness’ or ‘sample variance’. That is, values of σ within these lines could result simply from estimating σ over small (21-yr) windows of time. Note that σ always has a positive value. The confidence intervals were determined by shuffling the time series values, calculating the 21-yr running σ of the shuffled series, and repeating 5000 times. ‘Randomisation by shuffling’ is a useful statistical test because it makes no assumption about the statistical distribution of the data.

Time series filtering – Supplementary Table 3 and Supplementary Figure 6

To calculate the values in Supplementary Table 3, the *Data* series were filtered (using a Butterworth filter) into two time bands: Annual (11-13 months) and Interannual (24-96 months, equal to 2-8 years). Variance was calculated for the interannual (2-8 year) band extracted from the $\delta^{18}\text{O}$ *Data* series.

All *Data* series were regressed on the bandpass series, in order to calculate the percentage of variance explained by each bandpass series. These calculations were also repeated using an Interannual band of 24-84 months (2-7 years), which made little or no difference to the results in Supplementary Table 3. Annual to interannual variance ratios were calculated and plotted in Supplementary Figure 6.

Supplementary Discussion

Are any results sensitive to the chronological (monthly) tie-point?

Our result, of a shift in the seasonal timing of El Niño events relative to the calendar year for the ~4.3 kyBP coral (Fig. 2d-e), is not dependent upon the choice of monthly tie-point. From the cluster analysis, the shape of (and the differences in shape) the mean El Niño event and the mean La

Niña event for each time series cannot be changed by shifting the monthly tie-point. Cluster analysis does not require that a time series has an absolute chronology; only a relative chronology is needed.

Similarly, the number of months between the peak in the mean annual cycle (Fig. 3a) and the peak in the mean El Niño events (Fig. 2) is not dependant on the choice of monthly tie-point. For the SST series and modern coral $\delta^{18}\text{O}$ stack there are ~5-6 months between these two peaks, where the mean annual cycle peaks in June-July (Fig. 2a), and the mean El Niño event peaks in November-December (Fig. 2d,e). The number of months between these two peaks cannot be changed by shifting the monthly tie-point by ± 1 month because if the monthly tie-point is shifted from February, the corresponding peaks related to the mean annual cycle and the El Niño peak are shifted by the same amount, and the number of months between the peaks is maintained. This also applies to the ~4.3 kyBP fossil coral, where we see a delay (relative to today) of the peak in El Niño and La Niña events.

Are the changes in ENSO variance a consequence of internal variability?

Although ENSO variance in the ~4.3 kyBP coral is reduced relative to the present day it may still result from internal variability within the climate system. We test the likelihood of this situation using three tests: an AR(1) test for stochastic variability, and tests of ENSO variance against the simulated ENSO variance in two unforced pre-industrial climate system model control simulations: one from GFDL CM2.1 (Wittenberg, 2009), and the other from CSIRO Mk3L version 1.2 (Phipps and Brown, 2010; Phipps et al., 2011, 2012).

Part 1 – Autoregression test for stochastic variability

This test explores whether the ~4.3 kyBP coral has variance that could be produced from the statistics and dynamics of ENSO ‘as we know it’ for the present day. In this test coral variance is assumed to be an autoregressive (AR(1)) process forced by ENSO (as we know it) and by stochastic (internal) variability. That is, the system is driven by noise processes (generally high-frequency) and feedbacks within the system ‘reddden’ these processes, generating low frequency variations. For example, on long timescales (e.g. centennial) variability in the Pacific Ocean could be due to feedback processes that redden atmospheric noise and ENSO, resulting in more low frequency (decadal) variability than there would otherwise have been. In another example, the low frequency variance in corals could be present because the corals themselves are “climate integrators that redden ENSO” (Newman et al., 2003; Ault et al., 2009). The autoregression test we perform asks what range of standard deviations are possible with a stochastic model of ENSO (as we know it), and if the standard deviation in the ~4.3 kyBP coral ENSO is outside this range.

A second issue when carrying out this test is whether or not the ~4.3 kyBP time series is long enough. If a sampling window is taken from a system that has low frequency variations, and the sampling window is too short, then that window can represent higher or lower variance than the system mean but can still be within the range generated from the stochastic variability. We test whether the ~4.3 kyBP coral variance happens to be within the range of the stochastic model or whether it sits outside the stochastic model range of what can be generated from an autoregressive process.

These ideas were tested by viewing coral $\delta^{18}\text{O}$ as an autoregressive (AR(1)) process forced by both ENSO and stochastic variability (and with feedbacks ‘reddening’ the system):

$$\delta^{18}O_t = a\delta^{18}O_{t-1} + bN34_t + e_t \quad (3)$$

where $\delta^{18}O$ and N34 are anomaly time series (i.e. detrended and deseasonalised) of the modern coral stack and the NINO3.4 index, respectively; e is the atmospheric noise (high frequency); a is a parameter that controls the strength of the feedback within the system; b scales between NINO3.4 and $\delta^{18}O$ units. Note the anomaly time series were also annually averaged using July-June years.

Step 1 – calibrating and simulating the ENSO system

Since the above model is a regression model with multiple predictors, the coefficients were estimated based on the modern coral $\delta^{18}O$ stack and the NINO3.4 Index for 1939-2007 using the standard techniques of multiple linear regression (Supplementary Table 6).

The next step was to simulate the above model over a long time period, since the NINO3.4 series are too short to generate a distribution of ENSO variance for the Autoregression test. The model terms (N34 and e) were simulated as follows:

N34: An AR(2) model was fitted to the N34 anomaly time series, and the fitted AR(2) model was used to generate a long pseudo-N34 time series. The noise term in this AR(2) simulation was generated by randomly sampling from the residuals of the fitted AR(2) model. Simulated N34 time series were shown to have approximately the same variance and spectrum as the observed NINO3.4 anomaly time series. The test was repeated using an AR(3) model to simulate the N34 term. AR(2) or AR(3) models are used to simulate long time series of ENSO since they generate interannual spectral peaks (Kestin et al., 1998; Burgers, 1999).

e: A long time series of the innovations (noise) in equation (3) was generated by randomly sampling from the residuals of the fitted equation (3) model.

Thus, using these two terms, the equation (3) model can be simulated over long time periods. The simulated model can be described as an AR(2) (or AR(3)) process which is ‘reddened’ by an additional AR(1) process. The equation (3) stochastic model was simulated over 20,000 years.

Step 2 – sampling the system and applying the test

The standard deviation was calculated for every 175-year non-overlapping time window for the simulated equation (3) stochastic model (histogram in Supplementary Fig. 7). The standard deviation of the Kiritimati coral stack (69 years, 1939-2007) falls within the distribution of the equation (3) stochastic model (Supplementary Fig. 7), which confirms that the stochastic model reflects ENSO ‘as we know it’. The standard deviation of the ~4.3 kyBP fossil coral however, falls well outside the stochastic distribution (Supplementary Fig. 7), and thus the ~4.3 kyBP fossil coral time series is unlikely to have been generated by a stochastic process in which atmospheric noise and ENSO ‘as we know it’ is reddened by another process. The test was repeated using an AR(3) model to simulate the N34 term, and showed that the standard deviation in the ~4.3 kyBP fossil coral was also significantly different than the standard deviations generated with the stochastic model (not shown). Overall, this autoregressive test lends substantial credibility to the idea that the reduced mid-

Holocene ENSO intensity was due to different boundary conditions in the mid-Holocene, and not due merely to linear stochastic variability of the modern system.

Part 2 – Quantitative data-model comparison

We compare XM35 ENSO variability against the simulated variability in two multi-millennial unforced climate system model control simulations: a 4000-year control simulation from the GFDL CM2.1 model (Wittenberg, 2009) and a 10,000-year pre-industrial control simulation from the CSIRO Mk3L model version 1.2 (Phipps and Brown, 2010; Phipps et al., 2011, 2012). Model NINO3.4 SST was extracted from each control simulation and filtered using a 2-8 year bandpass filter. ENSO variability was then estimated by taking the standard deviation, relative to the long term model average, for moving 175-year windows (1-year time step, July-June years) i.e. for each model the 175-yr window standard deviations were divided by the long-term mean standard deviation of the simulations. A probability density function of ENSO variance for each model was plotted. Both models show that ENSO is capable of century-to-century modulation due to unforced internal variability, with the amplitude of this modulation being similar for the two models.

The ~4.3 kyBP coral time series was then filtered using a 2-8 year bandpass filter. ENSO variability was estimated by taking the standard deviation of the ~4.3 kyBP coral and dividing by ENSO variability for the 'Line Island Holocene coral mean' (Supplementary Figure 8 lower axes). The 'Line Island Holocene coral mean' takes the Line Island modern and fossil coral data from Cobb et al. (2013) and the ~4.3 kyBP coral, applies a 2-8 year bandpass filter, and then calculates the standard deviation for each record. The mean standard deviation (ENSO variability) for all these individual records was taken as the 'Line Island Holocene coral mean'.

For the upper axes in Supplementary Figure 8 the 'Line Island Holocene coral mean' and the ~4.3 kyBP ENSO variability were scaled relative to the 1968-1998 CE interval. The 1968-1998 CE ENSO variability is taken as 100%. Cobb et al. (2013) quote a 42% average Holocene reduction in ENSO variance with respect to the 1968-1998 CE interval and adding the ~4.3 kyBP coral $\delta^{18}\text{O}$ data changes this estimate by <1%. A 1968-1998 CE baseline is not used for the model results because pre-industrial control simulations are analysed and these do not incorporate the effects of anthropogenic forcings, and the 1968-1998 CE interval is only a 30-year window, whereas the model results were calculated on 175-year windows.

In contrast to the model ENSO variance, the ~4.3 kyBP coral ENSO variability is clearly outside the model unforced internal variability range at greater than the 99% confidence level (Supplementary Figure 8). It is extremely unusual that an unforced model simulation could produce a 175-year period with variance as low as the variance in the ~4.3 kyBP coral. Furthermore, it would be difficult for a coral record to lie outside the range of model variability if the coral record had the same low variance but was shorter in length. Overall, the reduced ENSO variance in the ~4.3 kyBP coral is unlikely solely due to unforced internal variability, and combined with results from the autoregression test and the ~4.3 kyBP changes in the seasonal phasing of ENSO, suggests a forced component to the ENSO changes.

Negligible influence of $\delta^{18}\text{O}$ seawater on Kiritimati Island microatoll $\delta^{18}\text{O}$

We used coupled measurements of coral Sr/Ca and $\delta^{18}\text{O}$ to demonstrate that the 0.06‰ increase in the amplitude of the mean annual cycle of $\delta^{18}\text{O}$ for the ~4.3 kyBP Kiritimati coral is due to

increased SST seasonality in the middle Holocene, rather than a change in the $\delta^{18}\text{O}$ of seawater ($\delta^{18}\text{O}_{\text{sw}}$). At seasonal and interannual scales, $\delta^{18}\text{O}_{\text{sw}}$ may vary with precipitation, evaporation, upwelling and/or advection.

The Kiritimati microatoll Sr/Ca-SST was used to remove the temperature component from the coral $\delta^{18}\text{O}$ record and calculate the coral $\delta^{18}\text{O}$ residual ($\Delta\delta^{18}\text{O}$), an estimate of the contribution of $\delta^{18}\text{O}_{\text{sw}}$ to the coral $\delta^{18}\text{O}$ signal. Results for the modern microatoll XM22 show minor changes in $\Delta\delta^{18}\text{O}$ in non-El Niño years (Supplementary Fig. 9a). During the exceptionally strong El Niño event of 1997-1998 high rainfall lowered $\delta^{18}\text{O}_{\text{sw}}$, thus contributing to the coral $\delta^{18}\text{O}$ (Supplementary Fig. 9a).

A 30-year subset of the full ~4.3 kyBP fossil coral record was analysed for Sr/Ca and the Sr/Ca-SST and $\Delta\delta^{18}\text{O}$ calculated (Supplementary Fig. 9b). The seasonal-scale variations in the $\Delta\delta^{18}\text{O}$ record are even smaller than those in the modern coral record (maximum 0.08‰ (1 σ) for any 13-year interval in the fossil record compared to 0.10‰ (1 σ) for the 13-year modern record (El Niño years excluded; Supplementary Fig. 9), and the fossil record contains no $\Delta\delta^{18}\text{O}$ variations comparable to 1997-1998. In addition, the remarkable correlation between Sr/Ca and $\delta^{18}\text{O}$ ($R^2 = 0.56$ fossil; $R^2 = 0.60$ modern) strongly supports our conclusion of reduced ENSO variance and the dominance of the annual cycle 4,400-4,200 yBP (see also Supplementary Table 3).

The influence of $\delta^{18}\text{O}_{\text{sw}}$ on coral $\delta^{18}\text{O}$ is negligible in terms of our analysis of the annual cycle of $\delta^{18}\text{O}$ during non-El Niño years. We quantify this using the $\Delta\delta^{18}\text{O}$. The average amplitude of $\Delta\delta^{18}\text{O}$ (annual maxima minus minima) for the non-El Niño years in the modern coral is 0.03‰ (Supplementary Fig. 9a). This value represents the average contribution of seasonal changes $\delta^{18}\text{O}_{\text{sw}}$ to the amplitude of the annual cycle of coral $\delta^{18}\text{O}$ for the present day. For the ~4.3 kyBP coral, the average amplitude of $\Delta\delta^{18}\text{O}$ for the non-El Niño years is 0.06‰. Therefore, the contribution of seasonal changes in $\delta^{18}\text{O}_{\text{sw}}$ to the 0.06‰ increase in the amplitude of the $\delta^{18}\text{O}$ annual cycle for the ~4.3 kyBP Kiritimati coral is only ~0.03‰ (the difference between the average $\Delta\delta^{18}\text{O}$ values for non-El Niño years in the modern and fossil corals). The result is realistic because, in general, an increase in the amplitude of the annual cycle of SST in the tropical ocean-atmosphere system should be accompanied by a slight increase in the seasonality of rainfall (and $\delta^{18}\text{O}_{\text{sw}}$).

Test of the null hypothesis that “there is no difference between the fossil and modern coral annual cycle amplitudes”

We test if the amplitude of the average annual cycle in the WM_stack and the ~4.3 kyBP fossil corals are different. To test this, we first assume that the centred (mean-subtracted) modern and fossil coral time series are generated from the same process, and calculate the null probability distribution of the difference in the annual cycle amplitude *between* the two time series. In statistical parlance, we are bootstrapping the null hypothesis probability distribution of “no difference in the annual cycle amplitude of two time series”.

This bootstrap test needs to generate two time series which have the same theoretical annual cycle amplitude as each other. The first step is to concatenate *both* the modern and fossil coral time series into the same time matrix, with 12 columns (corresponding to months), and with rows corresponding to years. Data within a particular column (month) are assumed to come from the same probability distribution, but different columns can have different probability density function (pdf; for example, the pdf of the February column may be different from the pdf of the July column). Next, the data within each column are resampled (with replacement), and then the matrix is split back into two time series of the same length as the original modern (29 years) and fossil (175

years) coral series. Thus, the two bootstrapped time series are realisations of the same (assumed) annual cycle process and differ only in length. The amplitude of the annual cycle of both bootstrapped time series is calculated separately using regression with a monthly indicator matrix. The difference in the amplitude of the annual cycle is calculated as:

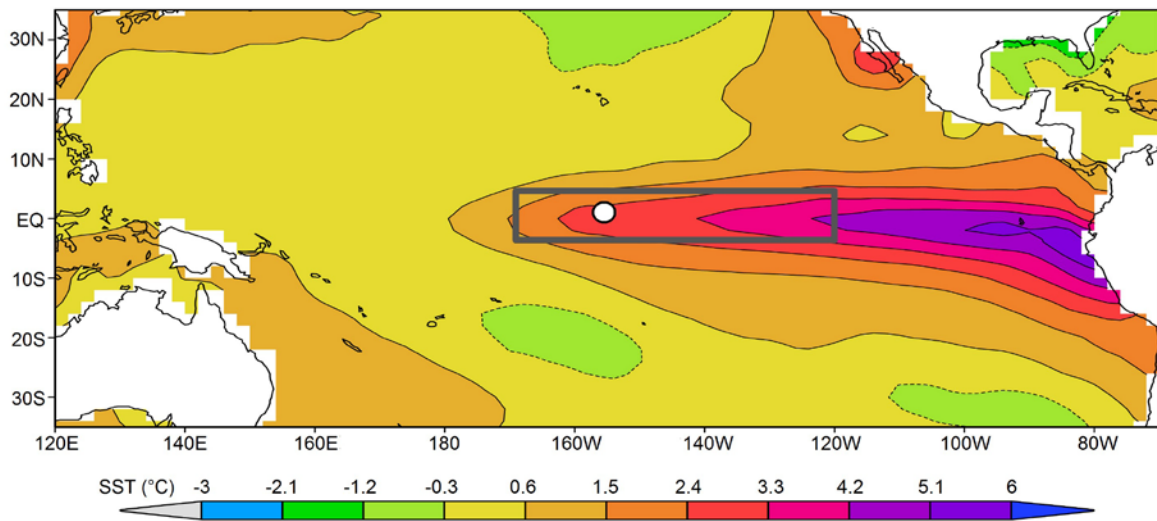
$$\text{Amplitude difference} = \text{Amplitude long time series} - \text{Amplitude short time series.}$$

2000 bootstrapped realisations of the annual cycle amplitude difference were generated, and are illustrated in Supplementary Figure 10.

As expected, the null hypothesis probability distribution varies around zero, because if the null hypothesis were true the annual cycle amplitude difference between the pairs of bootstrapped time series should be \sim zero. The pdf is also slightly skewed, because the amplitude of the 175-year long time series will be less varied than the amplitude of the 29-year time series, over a large number of bootstrapped realisations.

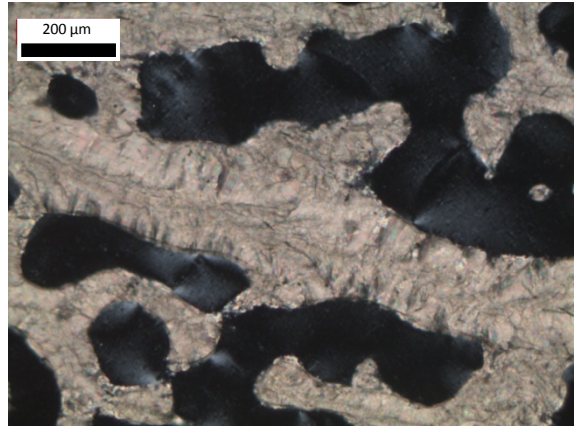
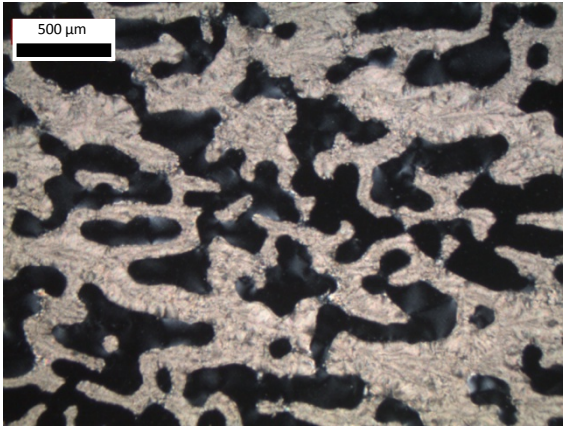
A one sided statistical test was used to quantify the annual cycle amplitude difference between the \sim 4.3 kyBP and modern corals, relative to the null hypothesis. A one-sided statistical test is used because we are interested if the observed annual cycle difference (fossil-modern) is relatively large. The probability distribution function shows that the one-sided 95% confidence interval on annual amplitude difference is 0.034‰ (Supplementary Fig. 10). The amplitude difference between the \sim 4.3 kyBP coral and the WM_stack is 0.05‰ (0.22-0.17=0.05‰) and therefore exceeds the 95% confidence limit of the one-sided test, which suggests that the observed difference between the annual cycle amplitude in XM35 and WM_stack is unusually large.

Supplementary figures

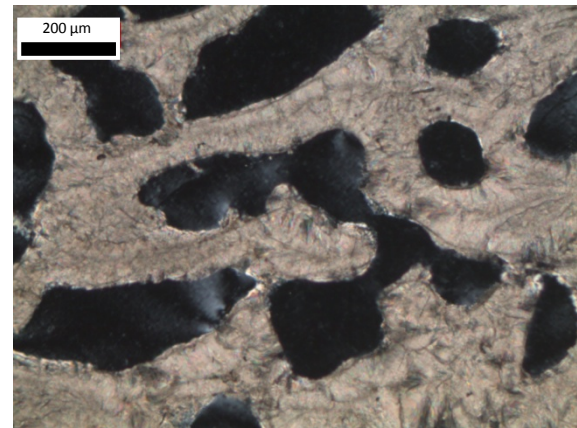


Supplementary Figure 1. Map of equatorial Pacific SST anomalies showing the location of Kiritimati Island. SST anomalies (ERSSTv3b; Smith et al., 2008) for December 1997 at the height of the 1997/1998 El Niño event. Kiritimati Island (white circle) is located within the NINO3.4 region (120-170°W, 5°N-5°S; grey box) and experiences warmer SSTs during El Niño events. Map created with the KNMI Climate Explorer (<http://climexp.knmi.nl/>).

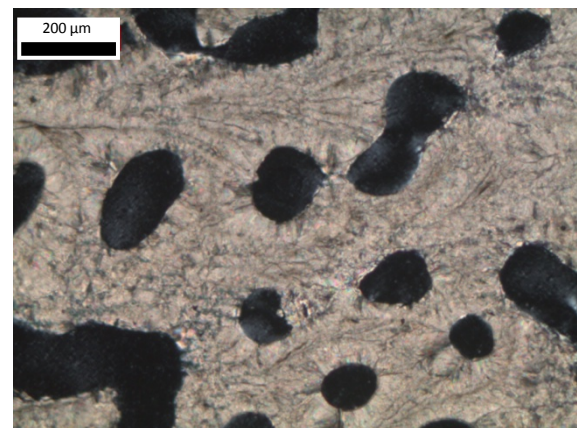
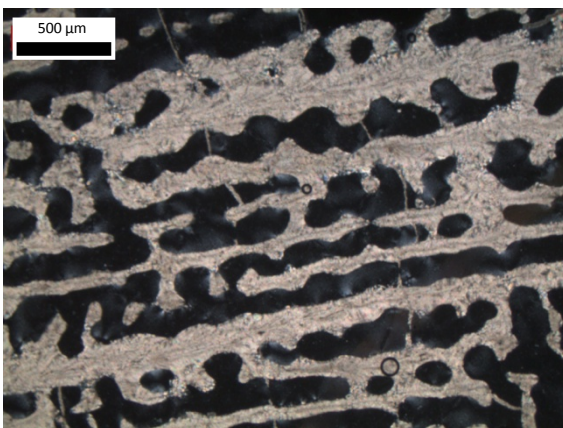
a XM35-D



b XM35-G

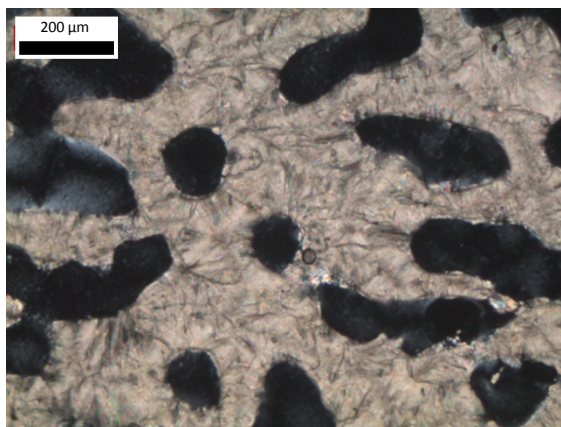
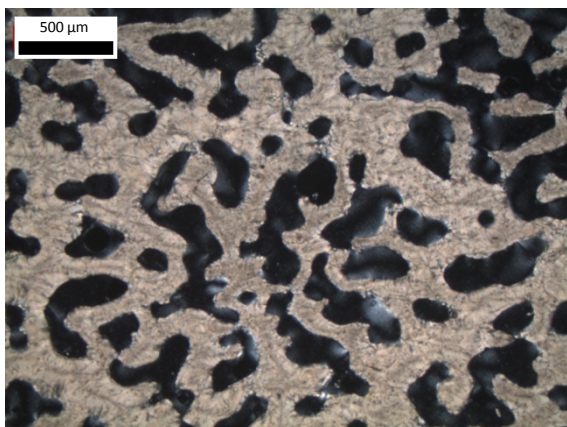


c XM35-H2

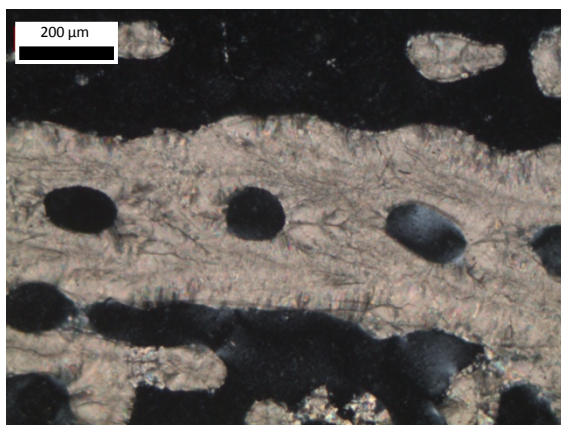
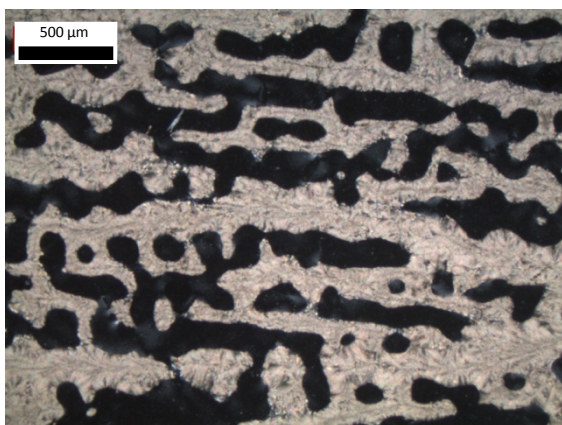


Supplementary Figure 2. Thin section images of coral XM35. XM35 coral slices **(a)** XM35-D, **(b)** XM35-G, **(c)** XM35-H2, **(d)** XM35-K, **(e)** XM35-M2, **(f)** XM35-O1, **(g)** XM35-P2, **(h)** XM35-R2, **(i)** XM35-S2, and **(j)** XM35-S2, as per the x-ray images in Supplementary Figure 3. All images are in cross polarised light. Images (a-f) and (h-i) show excellent preservation of centres of calcification and sclerozones, with no evidence of void filling or alteration by calcite or secondary aragonite. Image (g) shows evidence of minor dissolution along centres of calcification present in the XM35-P2 thin section. Image (j) shows evidence of rare dissolution along centres of calcification, observed in one part of the XM35-S2 thin section (excellent preservation in the rest of the thin section as shown in (i)).

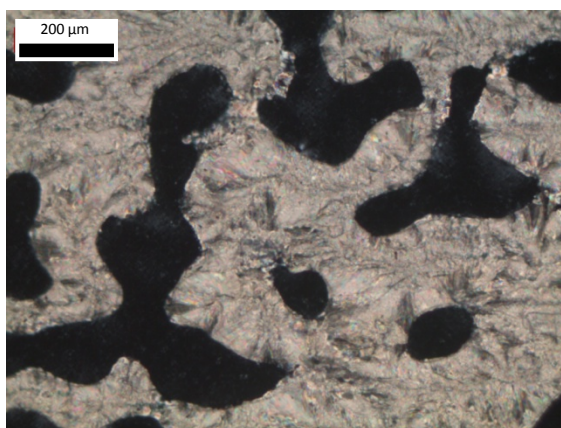
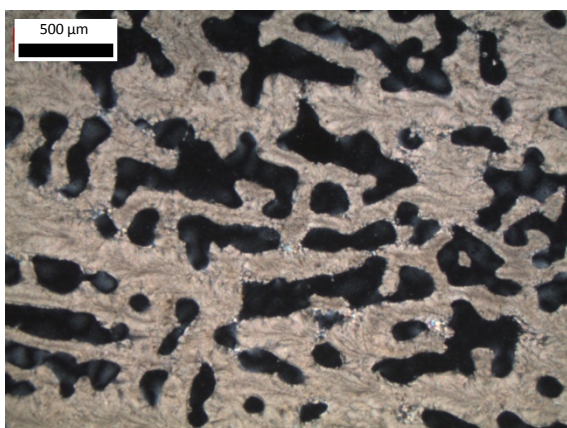
d XM35-K



e XM35-M2

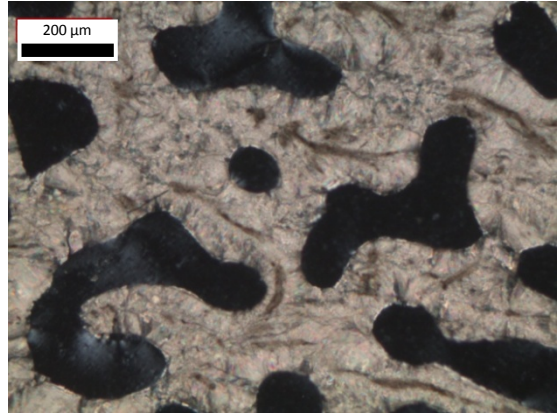
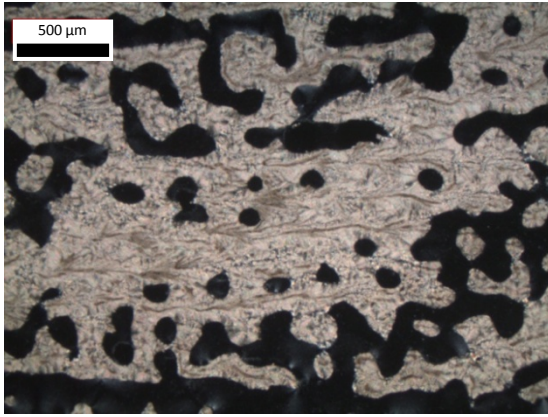


f XM35-O1

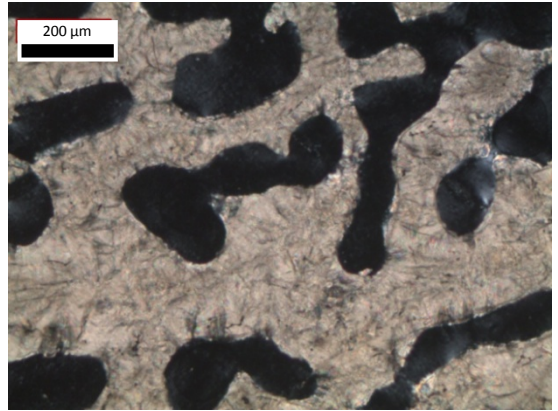
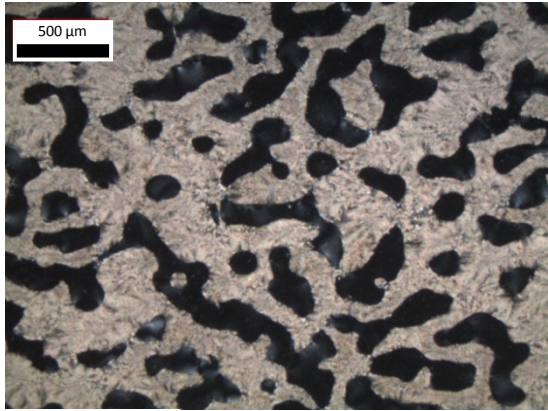


Supplementary Figure 2. continued.

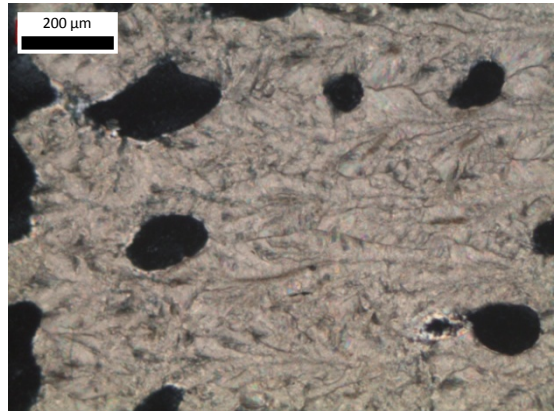
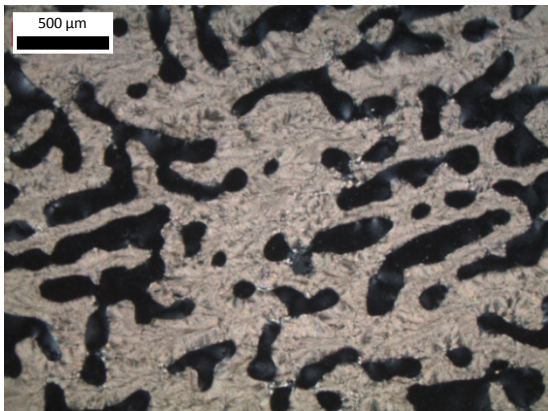
g XM35-P2



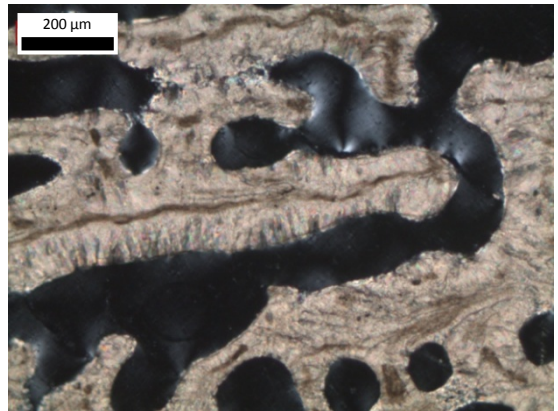
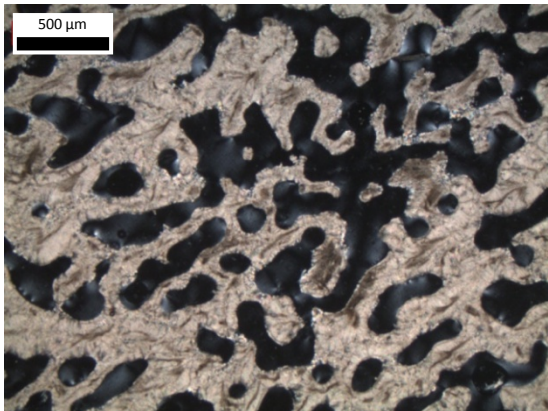
h XM35-R2



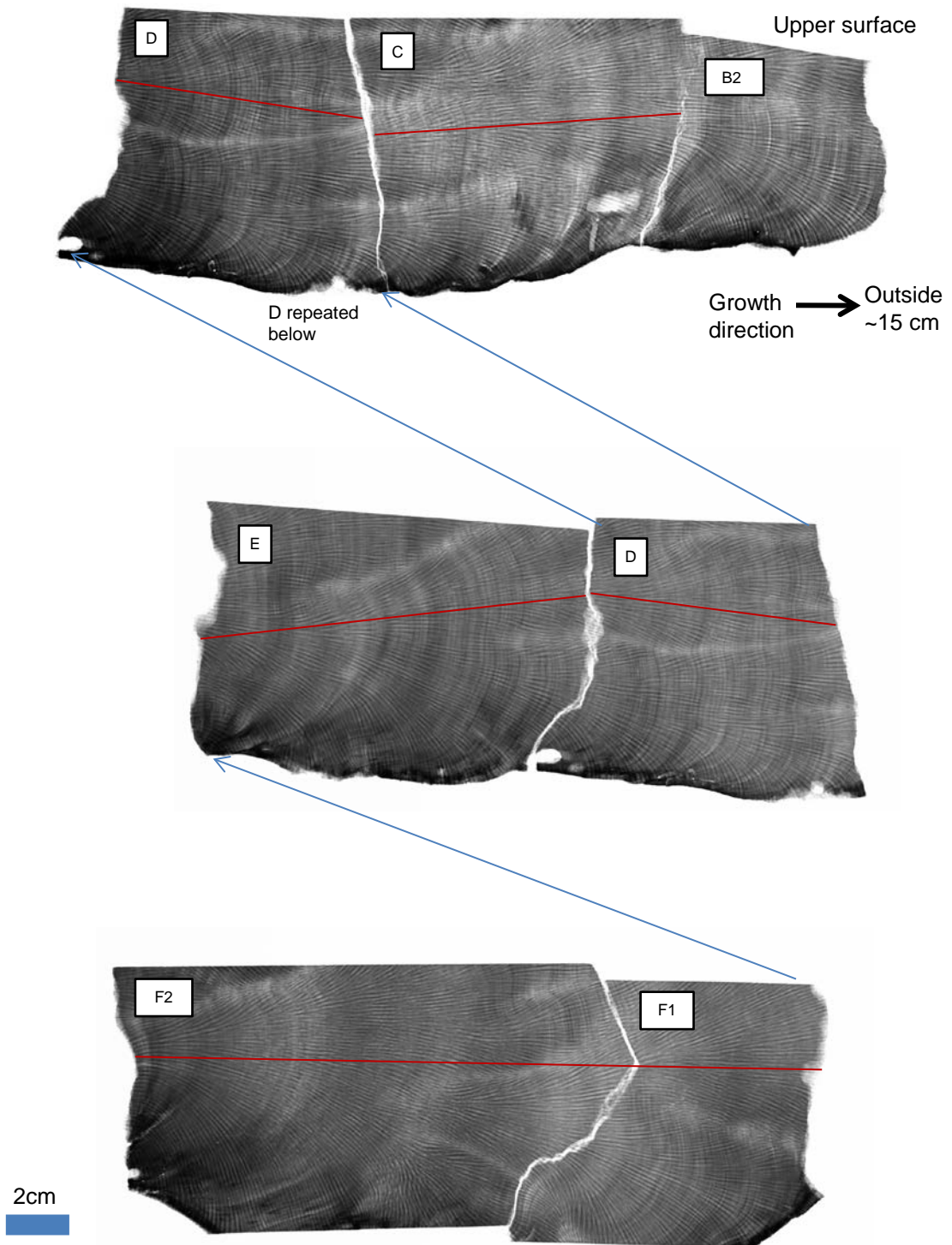
i XM35-S2



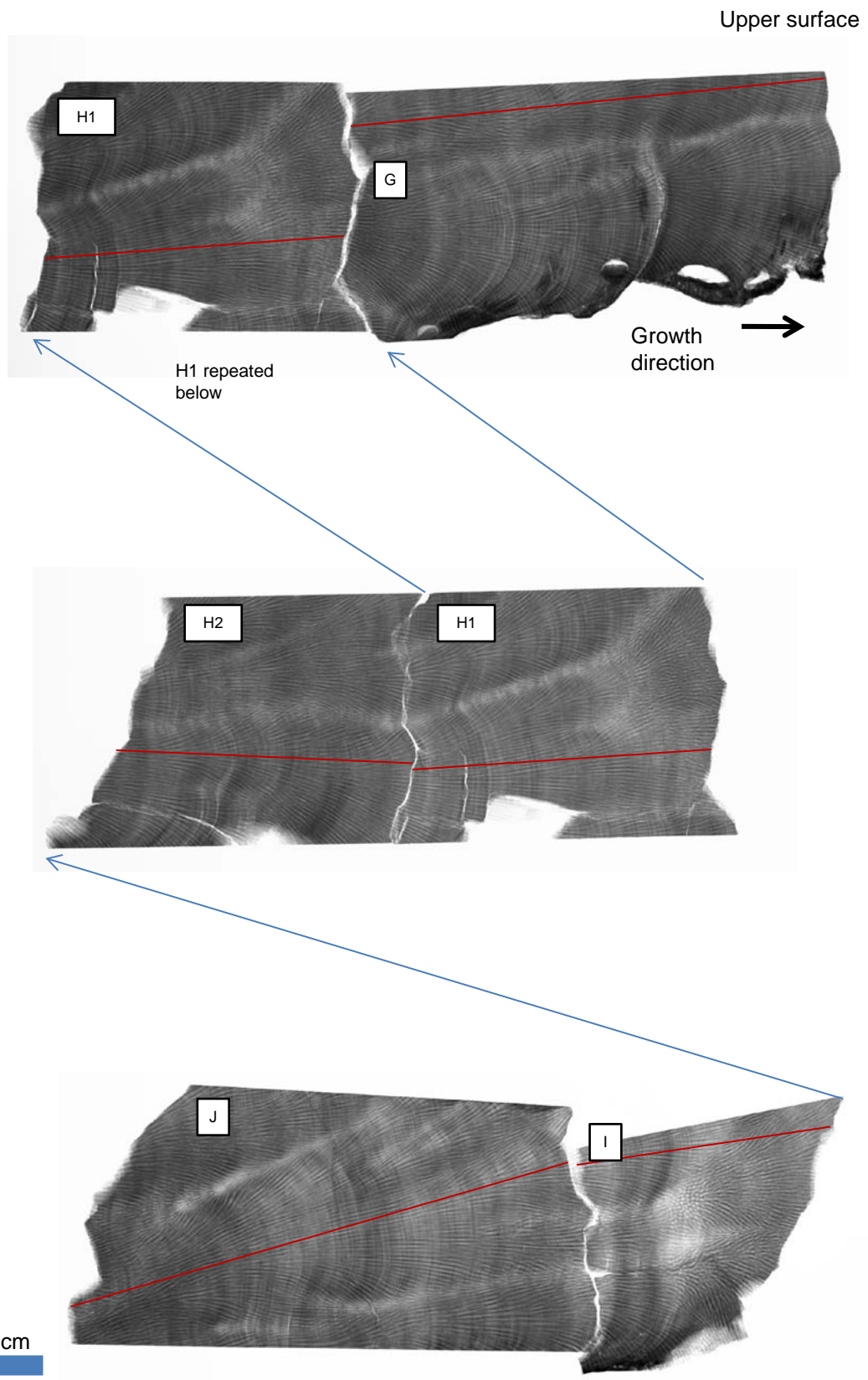
j XM35-S2



Supplementary Figure 2. continued.

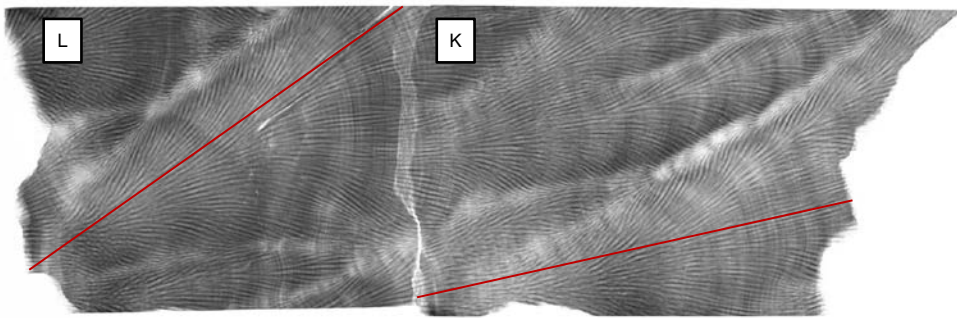


Supplementary Figure 3. X-radiograph of coral XM35. The letters indicate the slice label, with slice B2 closest to what was the living margin of XM35 (~15 cm from the former living margin). Slice S2 is furthest from the former living margin. The blue arrows indicate where the x-rays overlap and in some instances slices were x-rayed twice to facilitate ascertaining the maximum growth axis. Red lines indicate the sampling track along the maximum growth axis.

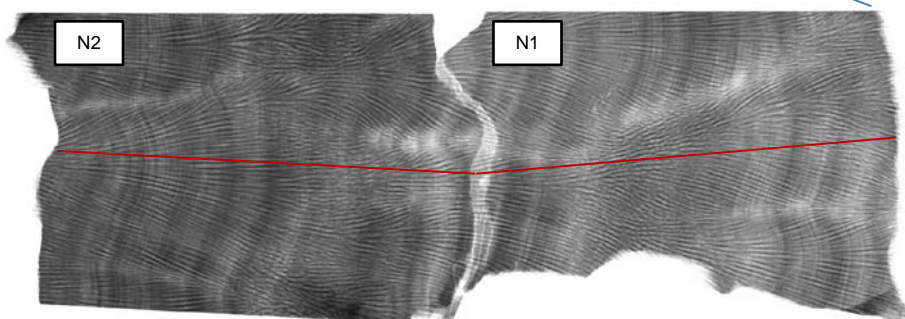
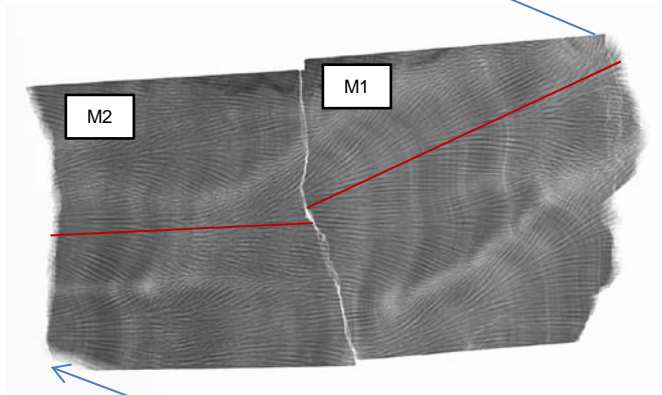


Supplementary Figure 3. continued.

Upper surface

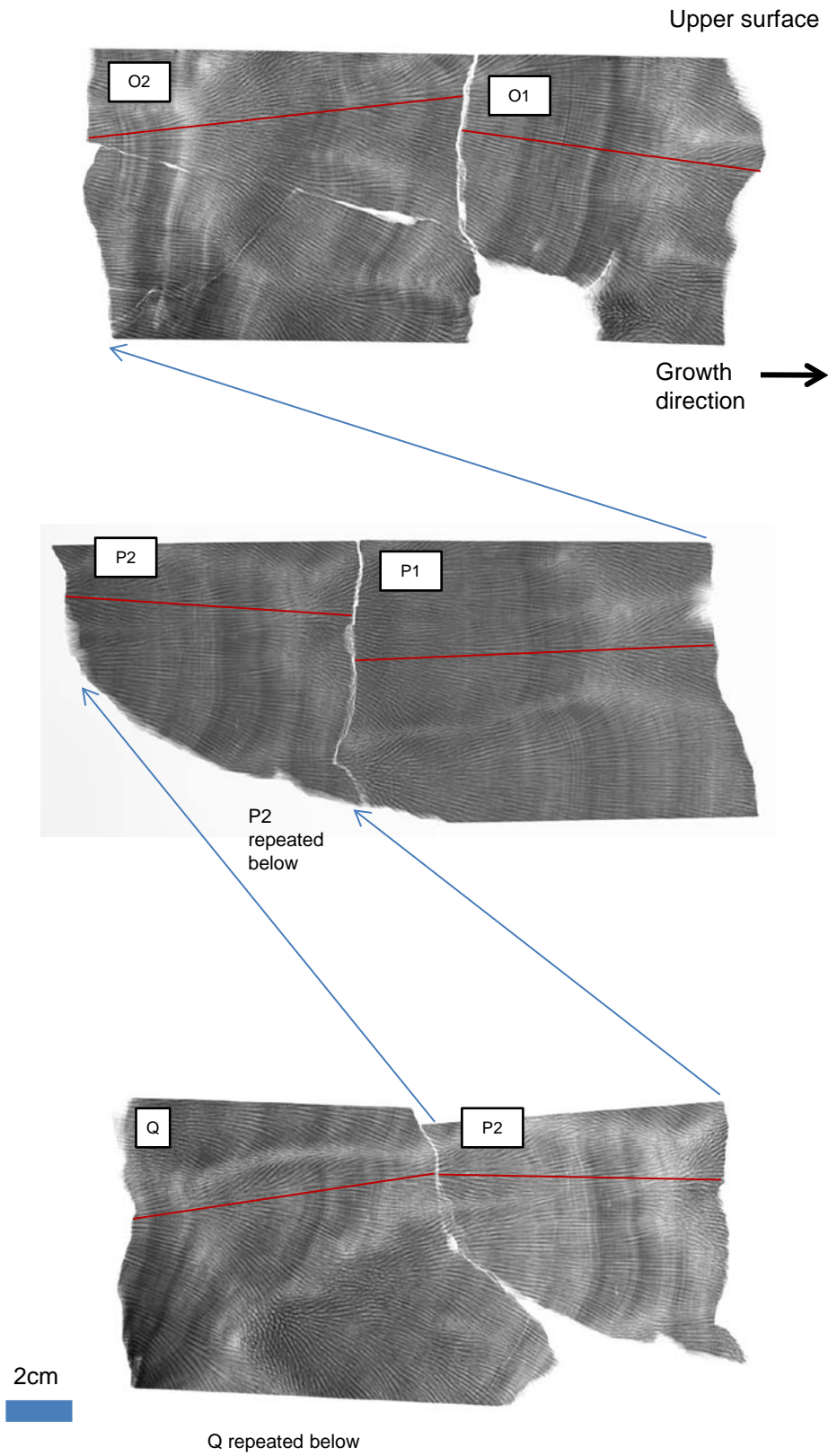


Growth direction →

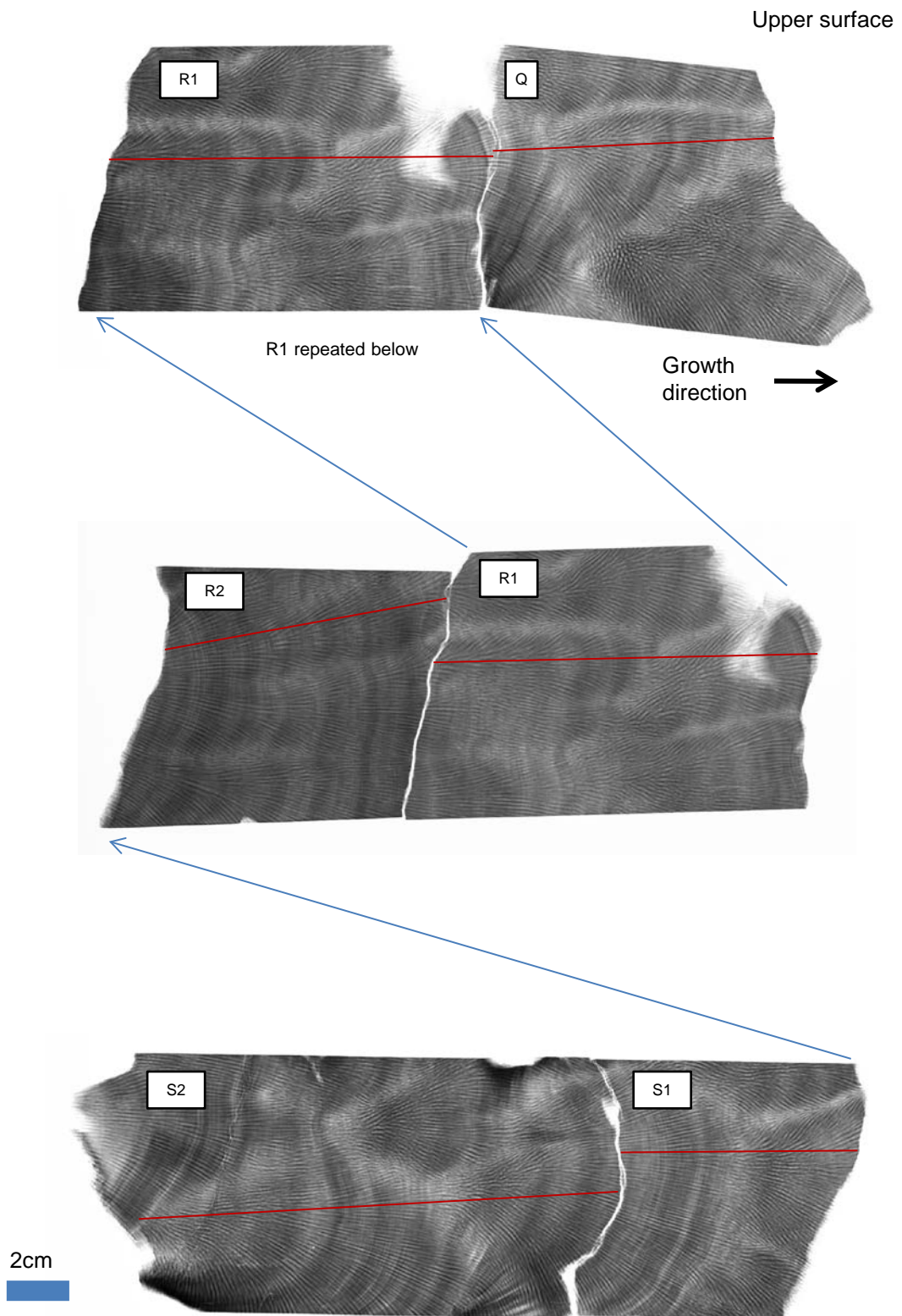


2cm

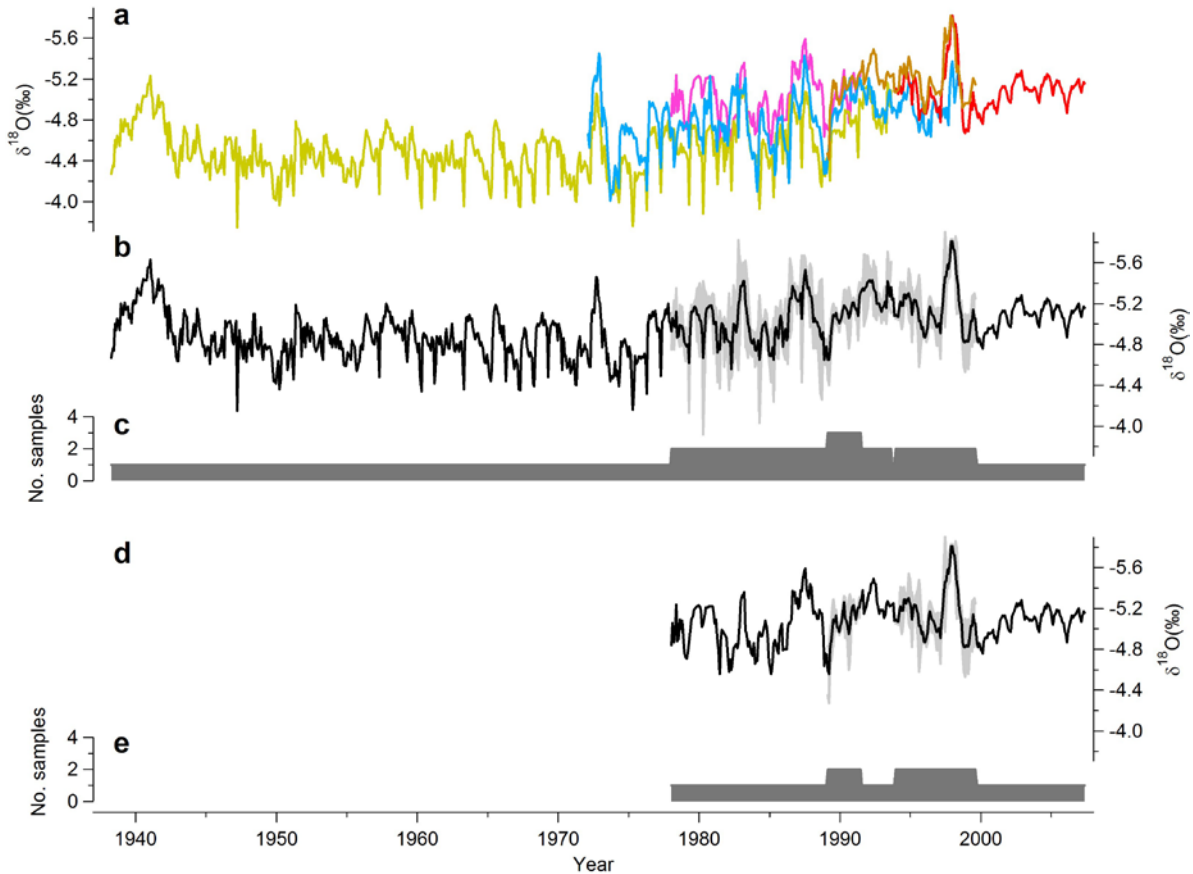

Supplementary Figure 3. continued.



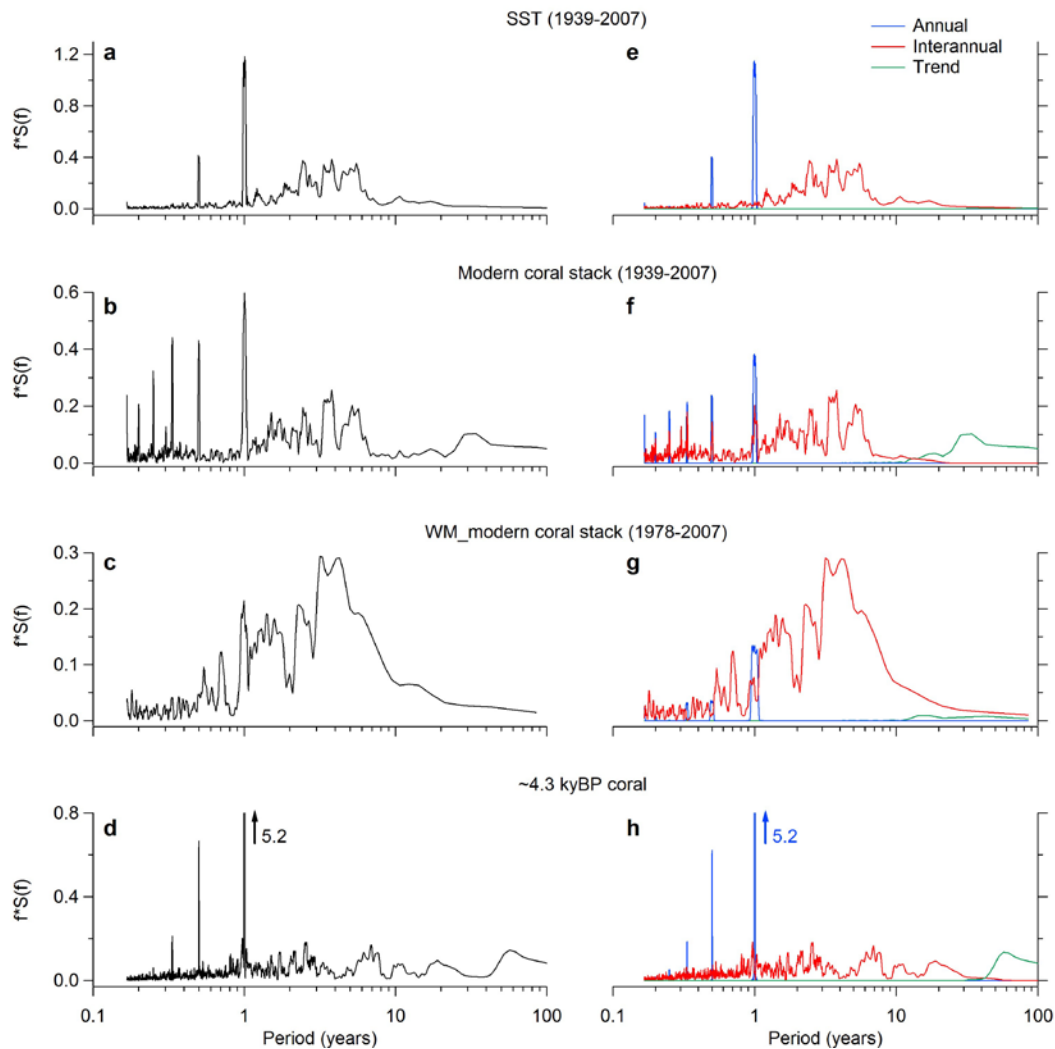
Supplementary Figure 3. continued.



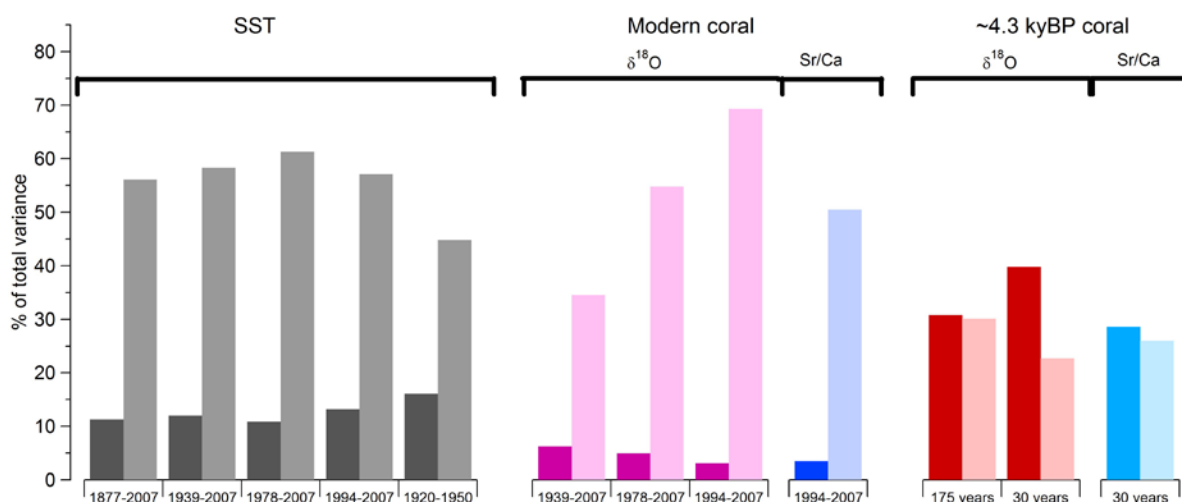
Supplementary Figure 3. continued.



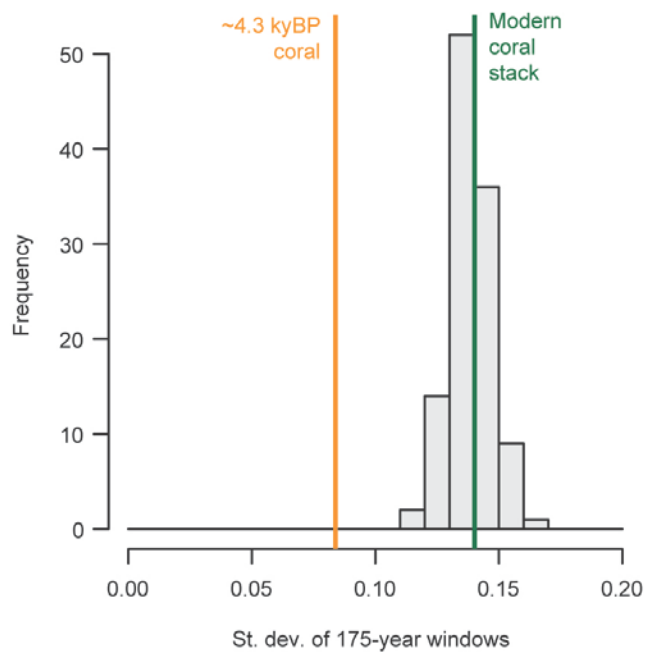
Supplementary Figure 4. Comparison of monthly $\delta^{18}\text{O}$ records for Kiritimati Island corals and construction of the modern coral $\delta^{18}\text{O}$ stack. **(a)** $\delta^{18}\text{O}$ records for March 1938 to May 2007 from Evans et al. (light green; 1998), Woodroffe et al. (pink, tan; 2003), Nurhati et al. (blue; 2009), and McGregor et al. (red; 2011a). The McGregor et al. (2011a) record is the average of six individual $\delta^{18}\text{O}$ transects from one coral microatoll (see McGregor et al. 2011a for further details). **(b)** Stack of Evans et al. (1998), Woodroffe et al. (2003), and McGregor et al. (2011a) Kiritimati $\delta^{18}\text{O}$ records (black). The stack was created by averaging $\delta^{18}\text{O}$ values for time-equivalent months from the published Kiritimati Island coral records. 0.4‰ was added to the Evans et al. (1998) record such that the mean for 1978.042-1991.458 AD matched that of the Woodroffe et al. (2003) coral CW3 (pink line in (a)). The differences between the records may reflect variations in the $\delta^{18}\text{O}$ of seawater around Kiritimati Island of up to 0.39‰ (McGregor et al., 2011a). 95% confidence interval (shaded) based on the standard deviation of the mean for time-equivalent samples. The Nurhati et al. (2009) record was not included due to the presence of secondary aragonite within the coral skeleton (LaVigne et al., In press), which introduces uncertainties in reconstructions based on coral geochemical proxies (Hendy et al., 2007). **(c)** The number of coral $\delta^{18}\text{O}$ analyses that were averaged to give each monthly value for the modern coral $\delta^{18}\text{O}$ stack record. **(d)** Stack of Woodroffe et al. (2003), and McGregor et al. (2011a) Kiritimati $\delta^{18}\text{O}$ records (WM_stack; black). The WM_stack was created by averaging $\delta^{18}\text{O}$ values for time-equivalent months from Woodroffe et al. (2003) and McGregor et al. (2011a) Kiritimati Island coral records in (a). 95% confidence interval (shaded) based on the standard deviation of the mean for time-equivalent samples from WM_stack. **(e)** The number of coral $\delta^{18}\text{O}$ analyses that were averaged to give each monthly value for the WM_stack coral $\delta^{18}\text{O}$ record. Modern coral stack, WM_stack data are in the Appendix.



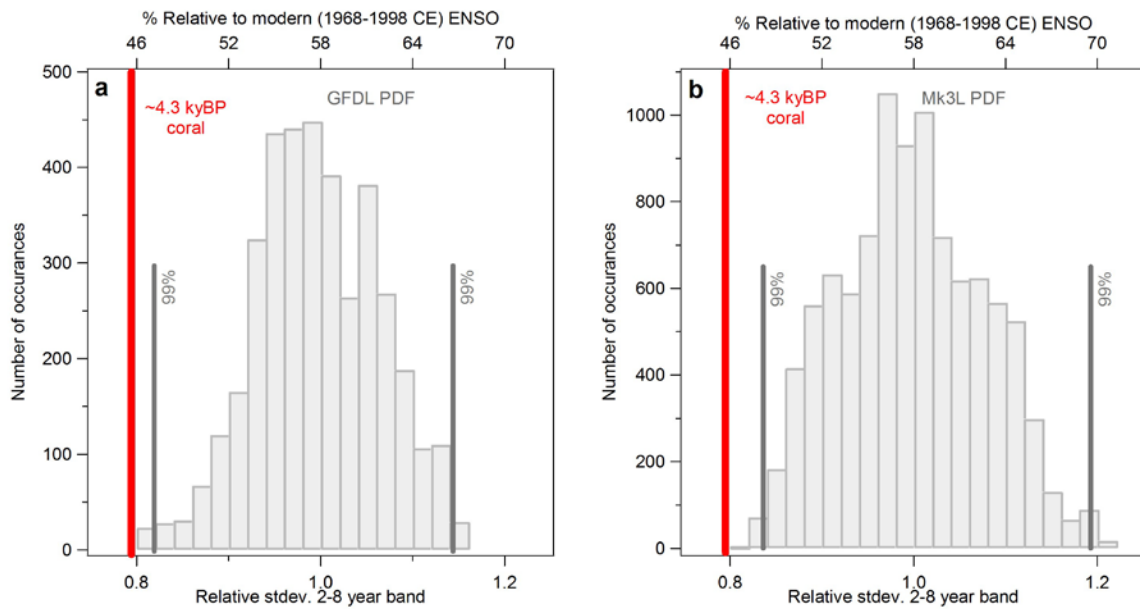
Supplementary Figure 5. Spectral analysis of Kiritimati SST and coral $\delta^{18}\text{O}$ records. Power spectra for **(a)** Kiritimati SST, **(b)** Kiritimati modern coral $\delta^{18}\text{O}$ stack, **(c)** WM_stack Kiritimati modern coral $\delta^{18}\text{O}$, and **(d)** XM35 $\delta^{18}\text{O}$. **(e-h)** *Trend* (green), *Annual* (blue), and *Residual* (interannual; red) components of the power spectra in (a-d). The *Data* series were initially scaled by their standard deviation. The component *Trend*, *Annual* and *Residual* series were scaled by the standard deviation of the *Data* series. Power spectra were then calculated using the multitaper method (see Methods for statistical calculations) and scaled by multiplying by frequency (which allows clearer comparison of the spectra of the different time series components). The spectral plots show that the *Trend*, *Annual* and *Residual* components occupy distinct frequency bands for each of the records used in this study. The *Residual* time series are dominated by variance in the interannual (2-8 year) band. Note that in the *Residual* time series of the modern coral $\delta^{18}\text{O}$ stack (1939-2007) the annual mean cycle is removed (as for all of the *Residual* time series) so the annual harmonics are due to the presence of irregular ‘spawning spikes’ from the Evans et al. (1998) record (compare plots (b) and (f) with (a) and (e), and (c) and (g); see also Supplementary Fig. 4). Note that the power spectra in Supplementary Figure 5 use the full record to demonstrate that the annual, interannual, and trend fall into distinct frequency ‘bins’, whereas the power spectra in Figure 1d are on the *Residual* (interannual) time series (i.e. detrended and deseasonalised) to highlight differences between the modern and fossil interannual power. In addition, the y-axis Supplementary Figure 5 is scaled by frequency, whereas the y-axis in Figure 1d is not.



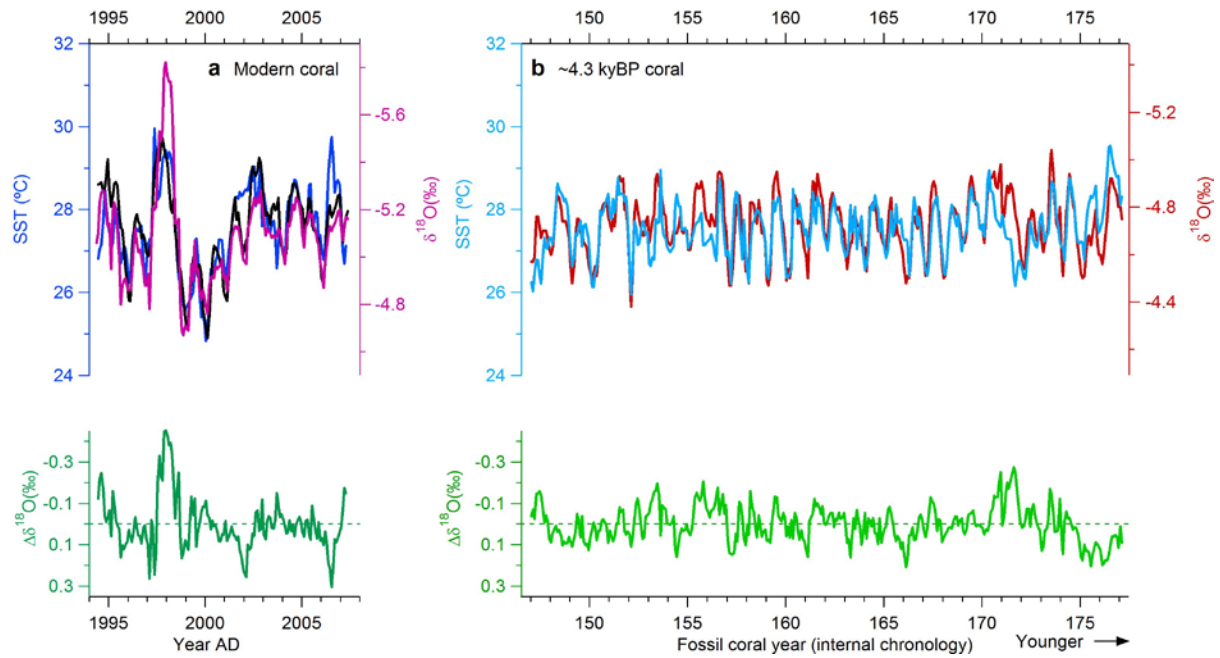
Supplementary Figure 6. Percentage of variance explained by the interannual and annual bands for Kiritimati SST and coral $\delta^{18}\text{O}$ and Sr/Ca records. Percentage of variance explained by the annual bands (dark coloured, left hand side column of each category pair) and interannual bands (light coloured, right hand side column of each category pair) are from Supplementary Table 3. The SST data are from ERSSTv3b (Smith et al., 2008) for the $2^\circ \times 2^\circ$ grid square centered on 158°W , 2°N , which includes Kiritimati Island, and the SST variance is calculated for intervals matched to the modern coral $\delta^{18}\text{O}$ and Sr/Ca, in addition to the full record. The $\delta^{18}\text{O}$ '1939-2007' category is for the modern coral stack data (Fig. 1 and Supplementary Fig. 4b), $\delta^{18}\text{O}$ '1978-2007' is for the WM_stack data (Supplementary Fig. 4d), and the $\delta^{18}\text{O}$ and Sr/Ca '1994-2007' category is for the XM22 modern coral (Supplementary Fig. 9a). For the ~ 4.3 kyBP fossil coral (XM35) the $\delta^{18}\text{O}$ '175 years' category is for the full ~ 175 -year long record (Fig. 1), and the '30 years' is for the 30 years of XM35 analysed for both $\delta^{18}\text{O}$ and Sr/Ca (Supplementary Fig. 9). Note the $\delta^{18}\text{O}$ '1939-2007' interannual variability is reduced compared to the other two modern coral $\delta^{18}\text{O}$ categories and the SST '1939-2007' category due to the multi-decadal variability and long term trend in $\delta^{18}\text{O}$ over this period (Supplementary Fig. 4a; Supplementary Fig. 5b and f). Overall, both the ~ 4.3 kyBP coral $\delta^{18}\text{O}$ and Sr/Ca records have a greater proportion of annual-scale variance relative to interannual variance than the modern coral records.



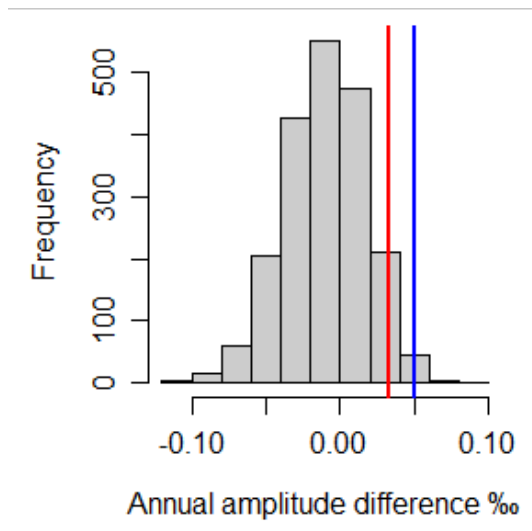
Supplementary Figure 7. Histogram of the distribution of standard deviations (of 175-year-long windows) generated using the stochastic model equation 3 (black) compared to the standard deviation of the Kiritimati coral $\delta^{18}\text{O}$ stack (green), and the standard deviation of the ~4.3 kyBP coral $\delta^{18}\text{O}$ record (orange).



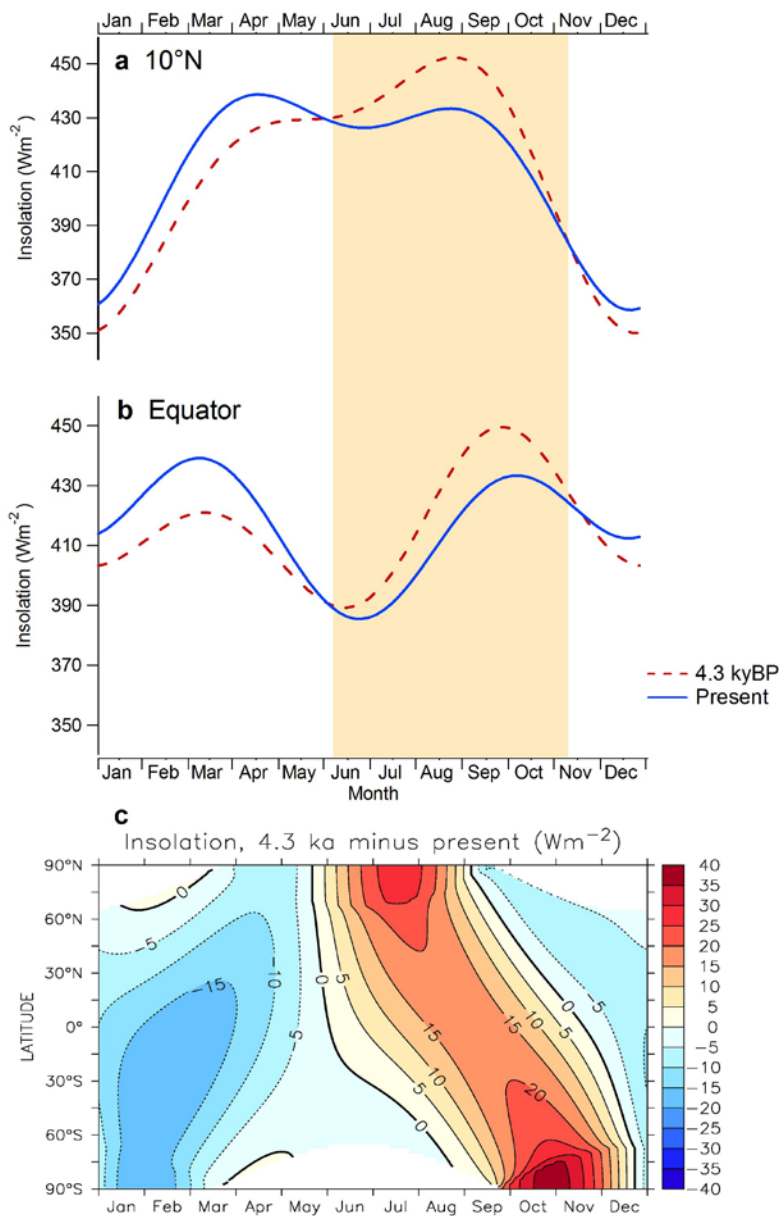
Supplementary figure 8. Probability density function for the standard deviation of 175-year windows of unforced pre-industrial climate system model control simulations of NINO3.4 ENSO variability compared to ENSO variance in the ~4.3 kyBP coral $\delta^{18}\text{O}$ time series. **(a)** ENSO variability in the GFDL CM2.1 model (Wittenberg, 2009) compared to the ~4.3 kyBP $\delta^{18}\text{O}$. **(b)** ENSO variability in the CSIRO Mk3L model version 1.2 (Phipps and Brown, 2010; Phipps et al., 2011, 2012) compared to the ~4.3 kyBP $\delta^{18}\text{O}$. In (a) and (b) grey bars are the probability density function of model NIÑO3.4 relative to the model mean, the grey line is the 99% confidence level for the model ENSO variability, and the red line is the ENSO variability in the ~4.3 kyBP coral $\delta^{18}\text{O}$ (lower y-axis). The upper x-axis is the ~4.3 kyBP coral ENSO variability relative to ENSO for the 1968-1998 CE interval. The upper axis does not imply that the ENSO variability from a modern coral (i.e. at 100%) is outside the model probably density function confidence limits. The upper axis modern coral baseline is based on a 30-year window (1968-1998) and is not directly comparable to the model results, which are calculated on 175-year windows.



Supplementary Figure 9. Comparison of Kiritimati microatoll $\delta^{18}\text{O}$, Sr/Ca-derived SST, and $\delta^{18}\text{O}$ residuals ($\Delta\delta^{18}\text{O}$). **(a)** Modern microatoll $\delta^{18}\text{O}$ (pink), Sr/Ca-SST (blue), ERSSTv3b SSTs (Smith et al. 2008) for 158°W , 2°N (includes Kiritimati Island; black), and the calculated $\Delta\delta^{18}\text{O}$ (dark green). **(b)** ~ 4.3 kyBP microatoll $\delta^{18}\text{O}$ (red), Sr/Ca-SST (light blue), and the calculated $\Delta\delta^{18}\text{O}$ (light green). Sr/Ca-SST was calculated using the calibration equation $\text{Sr/Ca-SST} = -12.056 \cdot \text{Sr/Ca} + 138.2681$ derived from reduced major axis regression of modern microatoll XM22 Sr/Ca and ERSSTv3b SSTs for 158°W , 2°N over the period 1994 to 2007. The Sr/Ca and ERSSTv3b show excellent correspondence ($R^2 = 0.64$). $\Delta\delta^{18}\text{O}$ was calculated using the centering method (Cahyarini et al., 2008) with a $\delta^{18}\text{O}$ -SST slope of $0.15\text{‰ per }^\circ\text{C}$ (McGregor et al., 2011a) and the Sr/Ca-SST slope above.



Supplementary figure 10. The difference in annual cycle amplitude of 2000 bootstrapped realisations of two time series with the same annual cycle process. The blue line is the observed annual cycle amplitude difference (fossil-modern coral). The red line is the 95% confidence limit for the one-sided test.



Supplementary figure 11. Comparison of insolation between 4,300 years ago and present. **(a)** Insolation for 4.3 kyBP (red dashed line) and present (blue line) at 10°N. **(b)** Insolation for 4.3 kyBP (red dashed line) and present (blue line) at the equator. **(c)** Difference in insolation between 4.3 ka and present for all latitudes. Orange shading in (a) and (b) highlights boreal late summer and early autumn when insolation at 4.3 kyBP is higher than present. Insolation data are from Berger (1978) and Berger and Loutre (1991). Data for (a) and (b) were accessed via Huybers (2006) <http://www.ncdc.noaa.gov/paleo/pubs/huybers2006b/huybers2006b.html> .

Supplementary tables

Supplementary Table 1. Summary of XRD analysis results for fossil coral microatoll XM35.

<i>Sample</i>	<i>Aragonite (%)</i>	<i>Calcite (%)</i>	<i>Chi squared</i>
XM35-D	99.9	0.1	1.85
XM35-G	100	0	1.85
XM35-H	99.8	0.2	1.73
XM35-H-2	100	0	1.78
XM35-K	100	0	1.86
XM35-M	99.8	0.2	1.69
XM35-M-2	99.9	0.1	1.93
XM35-O1	100	0	1.87
XM35-P2	99.8	0.2	1.97
XM35-R2	99.8	0.2	1.89
XM35-S2	99.9	0.1	2.49

Supplementary Table 2. Results from U-series dating of XM35 coral piece XM35-H1.

Sample wt.(g)	U (ppm)	$\pm 2s$	^{232}Th (ppb)	$\pm 2s$	$(^{230}\text{Th}/^{232}\text{Th})$	$\pm 2s$	$(^{230}\text{Th}/^{238}\text{U})$	$\pm 2s$	$(^{234}\text{U}/^{238}\text{U})$	$\pm 2s$	Uncorr. Age (ka)	$\pm 2s$	corr. Age (ka)	$\pm 2s$	corr. Initial $(^{234}\text{U}/^{238}\text{U})$	$\pm 2s$	Calendar age (cal yBP)
0.16916	3.2368	0.0020	0.48	0.002	913.01	4.28	0.0444	0.0001	1.1428	0.0010	4.321	0.010	4.317	0.010	1.1445	0.0010	4,256
0.16916	3.2543	0.0021	0.47	0.001	921.24	4.40	0.0441	0.0002	1.1430	0.0013	4.295	0.017	4.291	0.018	1.1447	0.0013	4,230
Weighted mean calendar age $\pm 2SE$ (cal yBP)																	
4,243 ± 9																	

Supplementary Table 3. Interannual band variance and percentage of total variance explained by the 2-8 year Butterworth band pass filter interannual and 11-13 month annual bands for Kiritimati Island SST and coral $\delta^{18}\text{O}$ and Sr/Ca records. See Supplementary Methods for calculations.

	Interannual band variance	Interannual band (% of total variance)	Annual band (% of total variance)	Ratio of interannual to annual bands
This study:				
SST ^a (1939-2007)	0.499 °C ²	58.3	12	4.9
Modern coral stack $\delta^{18}\text{O}$ (1939-2007)	0.0169 ‰ ²	34.5	6.22	5.54
SST ^a (1978-2007)	0.504 °C ²	61.3	10.9	5.61
WM_stack $\delta^{18}\text{O}$ (1978-2007)	0.0214 ‰ ²	54.8	4.96	11.1
SST ^a (1994-2007)	0.457 °C ²	57.1	13.2	4.33
XM22 $\delta^{18}\text{O}$ (1994-2007)	0.0247 ‰ ²	69.3	3.1	22.3
XM22 Sr/Ca (1994-2007)	0.00362 (mmol/mol) ²	50.5	3.49	14.5
SST ^a (1920-1950)	0.242 °C ²	44.8	16.1	2.78
SST ^a (1877-2007)	0.46 °C ²	56.1	11.3	4.97
~4.3 kyBP coral $\delta^{18}\text{O}$ (175 yrs)	0.0035 ‰ ²	30.1	30.8	1
~4.3 kyBP coral $\delta^{18}\text{O}$ (30 yrs)	0.00239 ‰ ²	22.7	39.8	0.57
~4.3 kyBP coral Sr/Ca (30 yrs)	0.000591 (mmol/mol) ²	26	28.6	0.909

^a ERSSTv3b (Smith et al., 2008) for the 2°x2° grid square centered on 158°W, 2°N, which includes Kiritimati Island.

Supplementary Table 4. Comparison of cluster analysis of NINO3.4 (ERSSTv3b) with five ENSO indices. For each ENSO event measure red shading indicates an El Niño event, white indicates no event, and dark grey shading indicate no data. Light pink indicates a lower level of certainty for events in the Meyers et al. (2007) classification.

Year	ENSO Indices					NINO3.4 Cluster analysis (this study)	% of ENSO Indices recording an event	Cluster NINO3.4 false positive/negative
	Meyers et al. 2007 ^a	BOM-SOI ^b	Trenberth 1997 ^c	IRI ^d	NOAA CDC ONI ^e			
1877	Red	Dark Grey	Dark Grey	Dark Grey	Dark Grey	Red	100	
1884	White	Dark Grey	Dark Grey	Dark Grey	Dark Grey	White	0	False positive
1885	White	Dark Grey	Dark Grey	Dark Grey	Dark Grey	White	0	False positive
1888	Red	Dark Grey	Dark Grey	Dark Grey	Dark Grey	Red	100	
1896	Red	Dark Grey	Dark Grey	Dark Grey	Dark Grey	Red	100	
1899	Red	Dark Grey	Dark Grey	Dark Grey	Dark Grey	Red	100	
1902	Red	Light Pink	Dark Grey	Dark Grey	Dark Grey	Red	100	
1904	White	White	Dark Grey	Dark Grey	Dark Grey	White	0	False positive
1905	Red	Red	Dark Grey	Dark Grey	Dark Grey	Red	100	
1911	Red	Red	Dark Grey	Dark Grey	Dark Grey	Red	100	
1913	White	Red	Dark Grey	Dark Grey	Dark Grey	White	50	
1914	Red	Red	Dark Grey	Dark Grey	Dark Grey	Red	100	
1918	Red	White	Dark Grey	Dark Grey	Dark Grey	Red	50	
1919	White	Red	Dark Grey	Dark Grey	Dark Grey	White	50	
1923	Red	White	Dark Grey	Dark Grey	Dark Grey	Red	50	
1925	Light Pink	Red	Dark Grey	Dark Grey	Dark Grey	Red	100	
1929	White	White	Dark Grey	Dark Grey	Dark Grey	White	0	False positive
1930	Red	White	Dark Grey	Dark Grey	Dark Grey	Red	50	
1939	White	Red	Dark Grey	Dark Grey	Dark Grey	White	0	False positive
1940	Red	Red	Dark Grey	Dark Grey	Dark Grey	Red	100	
1941	Red	Red	Dark Grey	Dark Grey	Dark Grey	Red	100	
1946	White	Red	Dark Grey	Dark Grey	Dark Grey	White	50	
1951	White	Red	Red	Red	Red	White	80	False negative
1953	White	White	Red	Red	Red	White	60	False negative
1957	Red	Red	Red	Red	Red	Red	100	
1958	White	White	White	White	Red	White	20	
1963	Red	Red	Red	Red	Red	Red	100	
1965	Red	Red	Red	Red	Red	Red	100	
1968	White	White	Red	Red	Red	White	50	
1969	White	Red	Red	Red	Red	White	80	
1972	Red	Red	Red	Red	Red	Red	100	
1976	White	White	Red	Red	Red	White	60	
1977	White	Red	Red	Red	Red	White	80	
1979	White	White	Red	Red	Red	White	20	
1982	Red	Red	Red	Red	Red	Red	100	
1986	Red	White	Red	Red	Red	Red	80	
1987	Red	Red	Red	Red	Red	Red	100	
1990	White	White	Red	Red	Red	White	20	
1991	Red	Red	Red	Red	Red	Red	100	
1993	White	Red	Red	Red	Red	White	60	False negative
1994	White	Red	Red	Red	Red	White	100	
1997	Red	Red	Red	Red	Red	Red	100	
2002	Dark Grey	Red	Dark Grey	Dark Grey	Dark Grey	Red	100	
2004	Dark Grey	White	Dark Grey	Dark Grey	Dark Grey	White	50	
2006	Dark Grey	Red	Dark Grey	Dark Grey	Dark Grey	Red	100	

^a Meyers et al. (2007) define an ENSO event as a year in which their ENSO index “was outside $\pm 1s$ for at least two consecutive months during the period from June to February”, where their ENSO index was calculated by an EOF analysis of 6 different ocean/atmosphere time series.

^b Australian Government Bureau of Meteorology Southern Oscillation Index where “sustained positive values of the SOI above +8 may indicate a La Niña event, while sustained negative values below -8 may indicate an El Niño event”. Data available from <http://www.bom.gov.au/climate/enso/enlist/> and <http://www.bom.gov.au/climate/enso/lnlist/>

^c Trenberth (1997) deems an event to occur “if 5-month running means of sea surface temperature (SST) anomalies in the Niño 3.4 region (5°N–5°S, 120°–170°W) exceed 0.4°C for 6 months or more”, using NINO3.4 data from NOAA and a base period from 1950-1979.

^d International Research Institute for Climate and Society (IRI) defines an El Niño or La Niña event “if the 5-month running-average of the NINO 3.4 Index exceeds +0.4 °C (for El Niño; -0.4 °C for La Niña) for at least 6 consecutive months” as applied to Kaplan SST data with a base period of 1951-1980. Available from <http://iri.columbia.edu/climate/ENSO/background/pastevent.html#list>

^e NOAA Climate Prediction Center Oceanic Niño Index (NOAA CPC ONI) threshold of “ +/- 0.5°C for the Oceanic Niño Index (ONI) [3 month running mean of ERSSTv3b SST anomalies in the Niño 3.4 region (5°N-5°S, 120°-170°W)], based on centered 30-year base periods updated every 5 years”. Events “are defined when the threshold is met for a minimum of 5 consecutive over-lapping seasons”. Data available from http://www.cpc.ncep.noaa.gov/products/analysis_monitoring/ensostuff/ensoyears.shtml

Supplementary Table 5. Comparison of cluster analysis of NINO3.4 (ERSSTv3b) with five ENSO indices. For each ENSO event measure blue shading indicates a La Niña event, white indicates no event, and dark grey shading indicate no data. Light blue indicates a lower level of certainty for events in the Meyers et al. (2007) classification.

Year	ENSO Indices					NINO3.4 Cluster analysis (this study)	% of ENSO Indices recording an event	Cluster NINO3.4 false positive/negative
	Meyers et al. 2007 ^a	BOM-SOI ^b	Trenberth 1997 ^c	IRI ^d	NOAA CDC ONI ^e			
1878							100	False negative
1879							100	
1886							100	
1889							100	
1890							100	False negative
1892							100	
1893							100	
1897							100	False negative
1903							100	
1906							100	False negative
1908							0	False positive
1909							100	
1910							100	
1916							100	
1917							100	
1922							50	
1924							100	
1928							100	False negative
1929							50	
1933							50	
1938							100	
1942							100	
1944							0	False positive
1949							100	
1950							100	
1954							100	
1955							100	
1956							50	
1964							100	
1967							20	False positive
1970							100	
1971							100	
1973							100	
1974							80	
1975							100	
1978							20	
1981							20	
1983							20	
1984							80	
1988							100	
1995							100	
1996							20	
1998							100	
1999							100	
2000							100	
2005							50	

^a Meyers et al. (2007) define an ENSO event as a year in which their ENSO index “was outside $\pm 1\sigma$ for at least two consecutive months during the period from June to February”, where their ENSO index was calculated by an EOF analysis of 6 different ocean/atmosphere time series.

^b Australian Government Bureau of Meteorology Southern Oscillation Index where “sustained positive values of the SOI above +8 may indicate a La Niña event, while sustained negative values below -8 may indicate an El Niño event”. Data available from <http://www.bom.gov.au/climate/enso/enlist/> and <http://www.bom.gov.au/climate/enso/lnlist/>

^c Trenberth (1997) deems an event to occur “if 5-month running means of sea surface temperature (SST) anomalies in the Niño 3.4 region (5°N–5°S, 120°–170°W) exceed 0.4°C for 6 months or more”, using NINO3.4 data from NOAA and a base period from 1950-1979.

^d International Research Institute for Climate and Society (IRI) defines an El Niño or La Niña event “if the 5-month running-average of the NINO 3.4 Index exceeds +0.4 °C (for El Niño; -0.4 °C for La Niña) for at least 6 consecutive months” as applied to Kaplan SST data with a base period of 1951-1980. Available from <http://iri.columbia.edu/climate/ENSO/background/pastevent.html#list>

^e NOAA Climate Prediction Center Oceanic Niño Index (NOAA CPC ONI) threshold of “ +/- 0.5°C for the Oceanic Niño Index (ONI) [3 month running mean of ERSST.v3b SST anomalies in the Niño 3.4 region (5°N-5°S, 120°-170°W)], based on centered 30-year base periods updated every 5 years”. Events “are defined when the threshold is met for a minimum of 5 consecutive over-lapping seasons”. Data available from http://www.cpc.ncep.noaa.gov/products/analysis_monitoring/ensostuff/ensoyears.shtml

Supplementary Table 6. Multiple linear regression diagnostics for equation (3) (Supplementary Discussion).

Coefficient	Estimate	Std. Error	t value	Pr(> t)
a	0.005055	0.050898	0.099	0.921
b	-0.183225	0.010364	-17.679	<2e-16 ***

*** p <0.001

Multiple R² = 0.83, F-statistic: 156.6 on 2 and 66 DF, p-value: < 2.2e-16

Supplementary references

- Adler, R.F., Huffman, G.J., Chang, A., Ferraro, R., Xie, P., Janowiak, J., Rudolf, B., Schneider, U., Curtis, S., Bolvin, D., Gruber, A., Susskind, J., Arkin, P., Nelkin, E.J., 2003. The Version 2 Global Precipitation Climatology Project (GPCP) monthly precipitation analysis (1979-present). *Journal of Hydrometeorology* 4, 1147-1167.
- Ault, T.R., Cole, J.E., Evans, M.N., Barnett, H., Abram, N.J., Tudhope, A.W., Linsley, B.K., 2009. Intensified decadal variability in tropical climate during the late 19th century. *Geophysical Research Letters* 36, L08602, doi:10.1029/2008GL036924.
- Berger, A., Loutre, M.F., 1991. Insolation values for the climate of the last 10 million years. *Quaternary Science Reviews* 10, 297-317.
- Berger, A.L., 1978. Long-term variations of daily insolation and Quaternary climatic changes. *Journal of the Atmospheric Sciences* 35, 2362-2367.
- Burgers, G., 1999. The El Niño stochastic oscillator. *Climate Dynamics* 15, 521-531.
- Cahyarini, S.Y., Pfeiffer, M., Timm, O., Dullo, W.-C., Schönberg, D.G., 2008. Reconstructing seawater $\delta^{18}\text{O}$ from paired coral $\delta^{18}\text{O}$ and Sr/Ca ratios: Methods, error analysis and problems, with examples from Tahiti (French Polynesia) and Timor (Indonesia). *Geochimica et Cosmochimica Acta* 72, 2841-2853.
- Cheng, H., Adkins, J., Edwards, R.L., Boyle, E.A., 2000. U-Th dating of deep-sea corals. *Geochimica et Cosmochimica Acta* 64, 2401-2416.
- Cobb, K.M., Westphal, N., Sayani, H.R., Watson, J.T., Di Lorenzo, E., Cheng, H., Edwards, R.L., Charles, C.D., 2013. Highly Variable El Niño–Southern Oscillation Throughout the Holocene. *Science* 339, 67-70, doi:10.1126/science.1228246.
- Evans, M.N., Fairbanks, R.G., Rubenstone, J.L., 1998. A proxy index of ENSO teleconnections. *Nature* 394, 732-733.
- Fang, Y., Chiang, J.C.H., Chang, P., 2008. Variation of mean sea surface temperature and modulation of El-Niño-Southern Oscillation variance during the past 150 years. *Geophysical Research Letters* 35, L14709, doi:10.1029/2008GL033761.
- Gagan, M.K., Chivas, A.R., Isdale, P.J., 1994. High-resolution isotopic records from corals using ocean temperature and mass-spawning chronometers. *Earth and Planetary Science Letters* 121, 549-558.
- Galbraith, R.F., Laslett, G.M., 1993. Statistical models for mixed fission track ages. *Nuclear Tracks and Radiation Measurements* 21, 459-470.
- Galbraith, R.F., Roberts, R.G., Laslett, G.M., Yoshida, H., Olley, J.M., 1999. Optical dating of single and multiple grains of quartz from Jinmium rock shelter, northern Australia: Part 1, experimental design and statistical models. *Archaeometry* 41, 339-364.
- Ghil, M., Allen, M.R., Dettinger, M.D., Ide, K., Kondrashov, D., Mann, M.E., Robertson, A.W., Saunders, A., Tian, Y., Varadi, F., Yiou, P., 2002. Advanced spectral methods for climatic time series. *Reviews of Geophysics* 40, 1-41, doi:10.1029/2001RG000092.
- Gilman, D.L., Fuglister, F.J., Mitchell, M., 1963. On the power spectrum of “Red Noise”. *Journal of the Atmospheric Sciences* 20, 182-184.
- Hartigan, J.A., Wong, M.A., 1979. A K-means clustering algorithm. *Applied Statistics* 28, 100-108.
- Hellstrom, J., 2003. Rapid and accurate U/Th dating using parallel ion-counting multi-collector ICP-MS. *Journal of Analytical Atomic Spectrometry* 18, 1346-1351.
- Hendy, E.J., Gagan, M.K., Lough, J.M., McCulloch, M., deMenocal, P.B., 2007. Impact of skeletal dissolution and secondary aragonite on trace element and isotopic climate proxies in *Porites* corals. *Paleoceanography* 22, PA4101, doi:10.1029/2007PA001462.
- Howell, P., Piasis, N., Ballance, J., Baughman, J., Ochs, L., 2006. ARAND Time-Series Analysis Software. Brown University, Providence RI.

- Huybers, P., 2006. Early Pleistocene glacial cycles and the integrated summer insolation forcing. *Science* 313, 508-511, doi:10.1126/science.1125249.
- Kestin, T.S., Karoly, D.J., Yano, J.-I., Rayner, N.A., 1998. Time-frequency variability of ENSO and stochastic simulations. *Journal of Climate* 11, 2258-2272.
- LaVigne, M., Nurhati, I.S., Cobb, K.M., McGregor, H.V., Sinclair, D., Sherrell, R.M., In press. Systematic ENSO-driven nutrient variability recorded by central equatorial Pacific corals. *Geophysical Research Letters*, doi:10.1002/grl.50765.
- Li, J., Xie, S.-P., Cook, E.R., Huang, G., D'Arrigo, R., Liu, F., Ma, J., Zheng, X.-T., 2011. Interdecadal modulation of El Niño amplitude during the past millennium. *Nature Climate Change* 1, 114-118, doi:10.1038/NCLIMATE1086.
- Ludwig, K.R., 2003. *Users Manual for Isoplot/EX 3.0: A Geochronological Toolkit for Microsoft Excel*. Berkeley Geochronology Center: Special Publication No. 4.
- McGregor, H.V., Abram, N.J., 2008. Images of diagenetic textures in *Porites* corals from Papua New Guinea and Indonesia. *Geochemistry Geophysics Geosystems* 9, Q10013, doi:10.1029/2008GC002093.
- McGregor, H.V., Fischer, M., Gagan, M.K., Fink, D., Woodroffe, C.D., 2011a. Environmental control of the oxygen isotope composition of *Porites* coral microatolls. *Geochimica et Cosmochimica Acta* 75, 3930-3944.
- McGregor, H.V., Hellstrom, J., Fink, D., Hua, Q., Woodroffe, C.D., 2011b. Rapid U-series dating of young fossil corals by laser ablation MC-ICPMS. *Quaternary Geochronology* 6, 195-206, doi:10.1016/j.quageo.2010.10.002.
- Meyers, G., McIntosh, P., Pigot, L., Pook, M., 2007. The Years of El Niño, La Niña, and Interactions with the Tropical Indian Ocean. *Journal of Climate* 20, 2872-2880, doi: 10.1175/JCLI4152.1.
- Moron, V., Vautard, R., Ghil, M., 1998. Trends, interdecadal and interannual oscillations in global sea-surface temperatures. *Climate Dynamics* 14, 545-569.
- Newman, M., Compo, G.P., Alexander, M.A., 2003. ENSO-forced variability of the Pacific Decadal Oscillation. *Journal of Climate* 16, 3853-3857.
- Nurhati, I.S., Cobb, K.M., Charles, C.D., Dunbar, R.B., 2009. Late 20th century warming and freshening in the central tropical Pacific. *Geophysical Research Letters* 36, L21606, doi: 10.1029/2009GL040270.
- Okai, T., Suzuki, A., Kawahata, H., Terashima, S., Imai, N., 2002. Preparation of a new Geological Survey of Japan geochemical reference material: Coral JCp-1. *Geostandards Newsletter* 26, 95-99.
- Paillard, D., Labeyrie, L., Yiou, P., 1996. Macintosh program performs timeseries analysis. *EOS Transactions AGU* 77, 379.
- Phipps, S.J., Brown, J.N., 2010. Understanding ENSO dynamics through the exploration of past climates. *IOP Conf. Series: Earth and Environmental Science* 9, 012010, doi:10.1088/1755-1315/9/1/012010.
- Phipps, S.J., Rotstayn, L.D., Gordon, H.B., Roberts, J.L., Hirst, A.C., Budd, W.F., 2011. The CSIRO Mk3L climate system model version 1.0 – Part 1: Description and evaluation. *Geoscientific Model Development* 4, 483-509, doi:10.5194/gmd-4-483-2011.
- Phipps, S.J., Rotstayn, L.D., Gordon, H.B., Roberts, J.L., Hirst, A.C., Budd, W.F., 2012. The CSIRO Mk3L climate system model version 1.0—Part 2: Response to external forcings. *Geoscientific Model Development* 5, 649-682, doi:10.5194/gmd-5-649-2012.
- Reynolds, R.W., Rayner, N.A., Smith, T.M., Stokes, D.C., Wang, W.J., 2002. An improved in situ and satellite SST analysis for climate. *Journal of Climate* 15, 1609-1625.
- Smith, T.M., Reynolds, R.W., Peterson, T.C., Lawrimore, J., 2008. Improvements to NOAA's historical merged land-ocean surface temperature analysis (1880-2006). *Journal of Climate* 21, 2283-2296.
- Soon-Il, A., 2009. A review of interdecadal changes in the nonlinearity of the El-Niño-Southern Oscillation. *Theoretical and Applied Climatology* 97, doi:10.1007/s00704-008-0071-z.

- Trenberth, K.E., 1997. The definition of El Niño. *Bulletin of the American Meteorological Society* 78, 2771-2777.
- Wittenberg, A.T., 2009. Are historical records sufficient to constrain ENSO simulations? *Geophysical Research Letters* 36, L12702, doi:10.1029/2009GL038710.
- Wood, S.N., 2006. *Generalized Additive Models: An Introduction with R*. Chapman and Hall/CRC Press.
- Woodroffe, C.D., McLean, R.F., 1998. Pleistocene morphology and Holocene emergence of Christmas (Kiritimati) Island, Pacific Ocean. *Coral Reefs* 17, 235-248.
- Woodroffe, C.D., Beech, M.R., Gagan, M.K., 2003. Mid-late Holocene El Niño variability in the equatorial Pacific from coral microatolls. *Geophysical Research Letters* 30, 1358, doi:10.1029/2002GL015868.
- Wyrtki, K., 1975. El Niño - The dynamic response of the equatorial Pacific Ocean to atmospheric forcing. *Journal of Physical Oceanography* 5, 572-584.
- Yu, J.-Y., Kim, S.T., 2011. Reversed spatial asymmetries between El Niño and La Niña and their linkage to decadal ENSO modulation in CMIP3 models. *Journal of Climate* 24, 5423-5434, doi: 10.1175/JCLI-D-11-00024.1.
- Zhou, H., Zhao, J., Qing, W., Feng, Y., Tang, J., 2011. Speleothem-derived Asian summer monsoon variations in Central China, 54–46 ka. *Journal of Quaternary Science* 26, 781-790.